Resonant Diffraction

Jean-Louis Hodeau,* Vincent Favre-Nicolin, Sandra Bos, Hubert Renevier, Emilio Lorenzo, and Jean-Francois Berar

Laboratoire de Cristallographie-CNRS, Associe a l'Université Joseph Fourier, 25 Avenue des Martyrs, BP 166, F-38042 Grenoble Cedex, France

Received November 14, 2000

Contents

I. Introduction

X-ray *resonant* (or *anomalous*) diffraction specificity is related to the close relationship between scattering, absorption, and refraction. *Resonant scattering* (or *dispersion*) refers to the modification of its intensity due to absorption processes involving interactions between the X-ray beam and the atoms in the sample. This interaction is dependent on electronic transitions from bound atomic orbitals. It contains the chemical and short-range order sensitivity of absorption as well as the long-range order sensitivity of diffraction. This enables *resonant diffraction* to be exploited for various structural studies ranging from pure crystallographic methods such as the structure factor phase determination by multiwavelength anomalous diffraction to pure spectroscopic ones such as diffraction anomalous fine structure.

Resonant diffraction is often called *anomalous diffraction*. This term finds its origin in the first research on light dispersion. For visible light, the index of refraction of transparent material generally increases as the wavelength decreases, and this corresponds to a *dispersion*, which was considered as "*normal*". However, near absorption bands, the slope of this index could be inverse versus the wavelength, and this was qualified as "*anomalous*" dispersion. This negative slope of the refraction index n versus wavelength λ is observed close to absorption edges, where dispersion effects are important and the term *anomalous scattering* is currently used for the absorption effects on X-ray scattering and optical properties. This phenomenon is not "*anomalous*" since the dispersion term exists for all wavelengths and all atoms, even if it is weaker far from absorption edges; thus, *resonant scattering* is certainly a more appropriate expression to qualify this process.

Before 1930, research on resonant scattering had little to do with structural applications. Rather it explored the properties of X-rays themselves and showed the complex nature of dispersion. For a long time the impact of resonant scattering and/or diffraction has been negligible for crystal structure determination and chemistry. The first structural application of resonant scattering tried to separate atoms of nearly equal atomic number.[1−3] However, the use of dispersion to obtain structural information on the stacking sequence of atoms in zinc blende had already been reported in 1930 in a contribution of Coster et al.[4] It was only in 1949 that Bijvoet[5] showed how to use this effect to solve the absolute configuration problem, which was a major application aimed to solve the absolute configuration of chiral molecules. The application of resonant diffraction to solve the phase problem in structure factor determination was also pointed out by Bijvoet,[5] but this method was

* To whom correspondence should be addressed. Phone: 33 4 76881142. Fax: 33 4 76881038. E-mail: hodeau@polycnrs-gre.fr.

10.1021/cr0000269 CCC: $36.00
Published on Web 05/30/2001

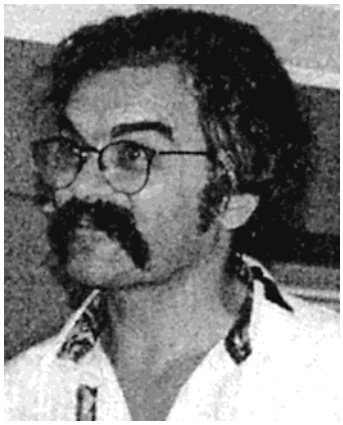

Jean Louis Hodeau was born in 1952 near Le Mans, France. He obtained his doctorate at the University of Grenoble in 1984. He has studied structural/physical property relationships in intermetallic magnetic/superconducting compounds and high-Tc superconductors and phase transformations of fullerenes under pressure/temperature. His initial interest was the study of ordered/disordered compounds using X-ray, electron, and neutron techniques. He now concentrates on the development of structural methods like the anomalous diffraction and DAFS analyses applied to powders, crystals, or multilayers. He is currently CNRS Research Director at the Laboratoire de Cristallographie, in charge of the Synchrotron Radiation Group involved on French CRG beam lines at the ESRF.

Vincent Favre-Nicolin was born in 1972 in Versailles, France. He studied chemistry in the Ecole Normale Supérieure in Paris, France. With J.-L Hodeau, at the CNRS Laboratoire de Cristallographie Grenoble, France, and at the ESRF, he completed his doctoral degree on the development of dispersive anomalous diffraction and its application to the structure determination of modulated structures and biological compounds. He is now working in the Laboratory of Crystallography in Geneva, Switzerland, on the development of object-oriented software for global optimization of crystal structures.

Sandra Bos was born in 1973 in Grenoble, France. She received her M.Sc. degree in 1996 and her Ph.D. degree in 1999 from the Université Joseph Fourier, Grenoble, France. She has contributed to the development of the anomalous X-ray diffraction technique and its application in the study of X-ray-absorbing samples. She works presently as an application engineer at a semiconductor company.

Hubert Renevier was born in 1963 near Grenoble, France. He received his M.Sc. degree in 1988 and his Ph.D. degree in 1991 from the Université Fourier, Grenoble. In 1993 he joined the Laboratoire de Cristallographie-CNRS, Grenoble, as Assistant Professor at the Joseph Fourier University. His Ph.D. and postdoctoral work focused on high-Tc superconductors; he is an active user of synchrotron radiation in large research facilities such as LURE, HASYLAB, and ESRF. He now develops the diffraction anomalous fine structure analysis and the use of the anisotropy of anomalous X-ray scattering in oxides, multilayers, and nanosystems.

not much used for this purpose since other methods, such as the *Patterson method* and much later the *direct methods*, were quite successful for crystallographic problems of that time.

Intensity variations as a function of energy above the absorption edge were reported in 1956 by Cauchois,[6] giving rise to "black lines" close to the absorption "white line" (Figure 1)**,** and were already interpreted as a consequence of a possible "anomalous" scattering contribution. In 1974, the status of theoretical and experimental resonant studies was reported at the Madrid conference on anomalous scattering[7] and showed that although the physical phenomenon was well understood, only a few applications on relatively simple problems were presented. The first large use of resonant diffraction was undertaken for macromolecular structural research. Although in the early days of protein crystallography resonant scattering was used to determine the absolute configuration of molecules and for phasing in association with isomorphous replacement, it was not until the 1980s and 1990s that a standard application of X-ray dispersion was found for MAD (multiwavelength anomalous diffraction) experiments. Clearly, the wide availability of tunable and intense X-ray synchrotron facilities was a key point for such a development as well as some theoretical, experimental, and computational advances. The International Conference on Anomalous Scattering in 1992 at Malente-Germany[8] showed the expansion of dispersion applications related to the use of synchrotron radiation. Developments ranged from the phase problem and crystal structure determinations to studies on anisotropy of resonant scattering, resonant Raman scattering, magnetic X-ray scattering, and nuclear resonant scattering.

J. Emilio Lorenzo was born in 1964 in Madrid, Spain. He received his M.Sc. degree in 1986 from the Universidad Autonoma de Madrid, Spain, and his Ph.D. degree in 1992 from Joseph Fourier University, Grenoble. In 1995 he joined the Laboratoire de Cristallographie, CNRS, Grenoble, and he is an active user of large European research facilities such as ILL and ESRF. He works in the field of quantum antiferromagnetism in low-dimensional compounds using neutron and X-ray scattering techniques, and his research interests also include neutron and anomalous X-ray scattering polarization techniques.

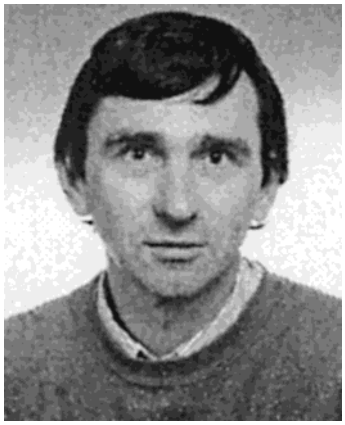

Jean-Francois Berar was born in 1949 in Moulins, France. He graduated as an engineer at the Ecole Centrale near Paris in 1972 and pursued his scientific studies in chemical physics. Working with Professor D. Weigel, he defended his thesis in Paris in 1980, concerning the disorder in organometallic crystals. Then he acted as Engineer in the Ecole Centrale Laboratory to promote powder diffraction. He was involved in incommensurate phases analysis. This led him to extend his expertise by using synchrotron light, and he joined LURE as Associate Researcher. In 1993, he joined the new French CRG beamlines at the ESRF and is now in charge of the anomalous material science CRG beamline, D2AM.

All resonant diffraction applications described herein are based on the contribution of the atomic scattering factor to the structure factor of Bragg reflections. The variation of the resonant scattering contribution near the edge of a given atom *a* induces a variation of the contribution of this specific atom to diffracted intensities. This property is used in several ways: (i) it allows element-selective diffraction experiments (contrast method) and (ii) it provides an elegant and efficient way of solving the structure factor phase problem for complex crystallographic structures like in biocrystallography (MAD method). On the other hand, the dispersive scattering contribution can be extracted from the diffracted intensities for a given atomic site or compound, so that diffraction and spectroscopy techniques can thus be combined (iii) to perform a site-selective spectroscopy by means of

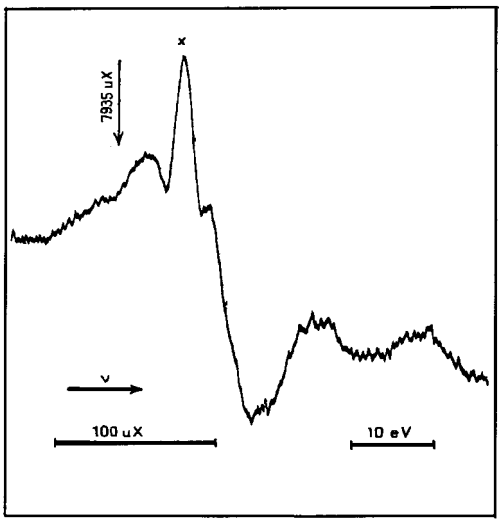

Figure 1. Spectral distribution of intensity of the (0 0 2) reflection of a "mica" analyzer with aluminum impurities. The black line "x" was already labeled anomalous or resonant scattering, and its contribution was different for the (0 0 1) reflection. (Reprinted with permission from ref 6. Copyright 1956 Elsevier Science.)

diffraction anomalous fine structure (DAFS method) or (iv) to use the anisotropy of anomalous scattering to extract information on site symmetry or distortion (AAS method). Resonant scattering also yields (v) an enhancement of the X-ray magnetic interaction by means of X-ray resonant magnetic scattering (XRMS method), which is used to probe both the electronic structure and the magnetic properties. In this contribution, after a recall of the resonant scattering process and of the properties of the resonant factors, we will present examples of these different applications.

II. Resonant Scattering

Scattering power is characterized for all particles by a scattering factor *f*. The scattering of X-rays from atoms comes from the interaction with electrons. The atomic scattering factor f_a is defined as the ratio of the amplitude of the wave scattered by the atom *a* to the amplitude of the wave scattered by a free electron. This term is complex ($f_a = f_{oa} + f_a' + if_a''$). Only the normal (nonresonant) form factor $f_{oa}(Q)$ is frequency or wavelength independent and is the Fourier transform of the electronic density, $\rho_a(r)$, in the atom. This real scattering factor f_{oa} decreases with increasing scattering vector Q ($|Q| = 4\pi \sin\Theta/\lambda$) or Bragg angle 2Θ. In the nonrelativistic approximation, it tends toward the atomic number Z_a in the forward scattering limit ($2\Theta = 0$). However, for heavy atoms, a relativistic correction (onf the order of $0-2$ e^-) must be subtracted.[9] This constant f_{oa} factor neglects electronic binding effects on the scattering process.

The complex part of the atomic scattering factor ($f_a'(\omega,Q) + if_a''(\omega,Q)$) is *the resonant scattering factor* which is sensitive to the X-ray photons that are absorbed by the photoelectric effect. When a photon with frequency ω, wavelength λ, or energy E ($\lambda = 2\pi c/\omega$, $E = \hbar\omega$, E (in eV) $= 12\,398.4/\lambda$ (in Å)) is

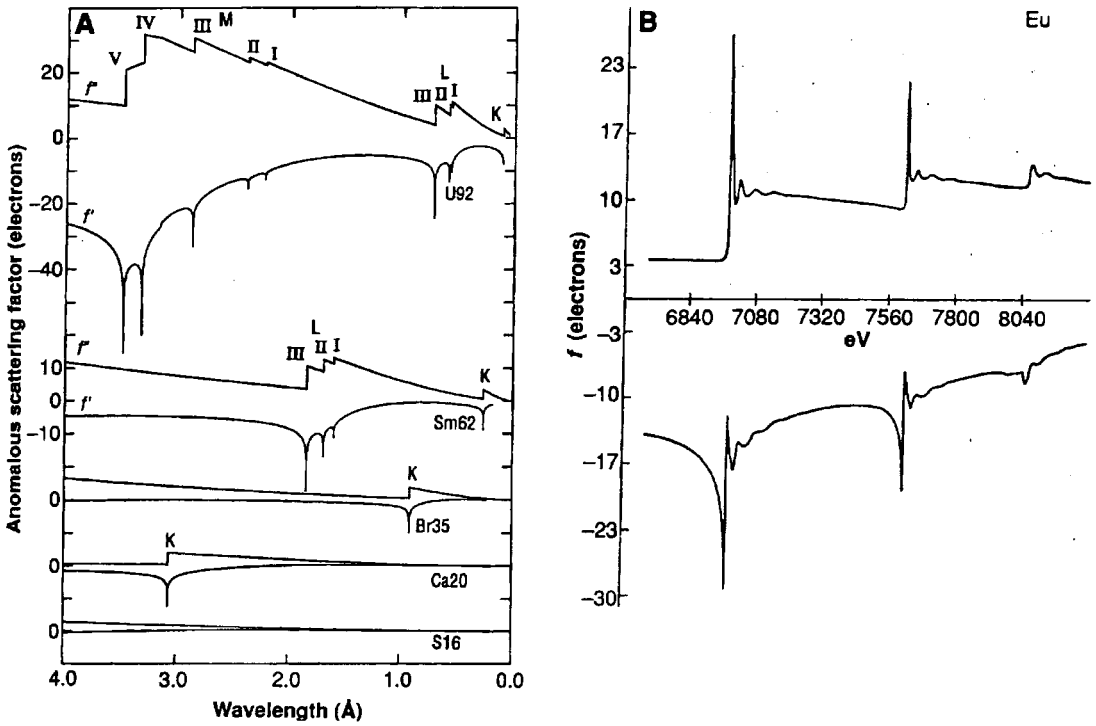

Figure 2. Variations of the anomalous atomic scattering factors f', f'' with λ or E near absorption edges. (Reprinted with permission from ref 14. Copyright 1991 American Association for the Advancement of Science.)

close to an electronic resonance, it can interact with the corresponding bound inner electron and be absorbed. The resonant term is therefore a complex quantity, which depends on the chemical nature of the scatterer and becomes substantial near the absorption edges of the scatterer. For X-rays, resonant effects are important for nearly all atoms.

Some results of classical optical theory[10] are recalled here. The index of refraction $n(\omega)$ is related to the scattering factor $f_a(\omega)$:($n(\omega) = 1 - (2\pi e^2/m\omega^2)\sum_a N_a f_a(\omega)$) and may be written as $n = 1 - \delta = 1 - \alpha - i\beta$, where α and β vary with the frequency or the wavelength and are, respectively, proportional to the real and imaginary part of the atomic structure factor. Since the refractive index is complex, the electromagnetic wave of frequency ω propagating in a medium of index n has the form $E = E_0 e^{i\omega(t-nr/c)} = E_0 e^{i\omega(t-(1-\alpha)r/c)} e^{-\beta\omega r/c}$ and the absorptive refraction term β is proportional to the linear absorption coefficient μ ($\beta = \mu c/2\omega$, $\mu(\omega) = (4\pi e^2/mc\omega)\sum_a N_a f_a''(\omega)$). The imaginary term $f_a''(\omega)$ is proportional to $\omega\mu_a(\omega)$, and the real term $f_a'(\omega)$ can be obtained from the real part of the refractive index $n(\omega)$. Furthermore, the causality relation between an applied field and its effect leads to the Kramers−Kronig relation between the real part $f_a'(\omega)$ and the imaginary part $f_a''(\omega)$ of the scattering factor ($f_a'(\omega) = (2/\pi)\int_0^\infty [\omega' f_a''(\omega')/(\omega^2 - \omega'^2)]d\omega'$, where the Cauchy principal value is taken for the integral).[11] This means that absorption and dispersion are intimately related and that we need only to measure either $f_a'(\omega)$ or $f_a''(\omega)$ to determine the other term.

A. Variation of f_a with the Scattering Angle

Because of the diffuseness of outer electron shells, the normal term f_{oa} decreases rapidly with $\sin\Theta/\lambda$. On the contrary, f_a'' and f_a' originate mainly from core electron transitions. Because the radius of inner absorbing electron shells (K, L,...) is much smaller than the wavelength of X-ray photons, f_a' and f_a'' anomalous terms do not vary significantly with the scattering angle 2Θ.[12] For example, anomalous diffraction experiments performed on Ni powder near the K edge have shown that f_{Ni}' has nearly the same value at different scattering angles (angular dependence $< 0.2e^-$, error $\sim 0.2e^-$).[13] Due to the decrease of f_{oa} with $\sin\Theta/\lambda$, resonant scattering terms are relatively more important at high 2Θ values (for reflections with high (hkl) indices).

B. Variation of f_a with the Energy

As $f_a''(E)$ is proportional to $E\mu_a(E)$, $f_a''(E)$ displays similar energy variations to the absorption coefficient $\mu_a(E)$. Since $f_a'(E)$ and $f_a''(E)$ are related by the Kramers−Kronig relation, $f_a'(E)$ also shows large variations with energy at the absorption edges (Figure 2).[14] This strong change of the resonant atomic scattering factor can be used for contrast experiments, and K or L absorption edges of almost all atoms are accessible between 3 and 40 keV with synchrotron radiation.

C. Chemical Sensitivity of f_a' and f_a''

Resonant scattering factors can be determined by theoretical calculations which give reliable values far from the absorption edges where damping and binding effects can be neglected.[15−18,9] However near edges μ_a, absorption spectra (and f_a'', f_a' ones) exhibit several features that are related to the chemical nature of the sample and its structure.

(i) For a given chemical state, some atoms exhibit a sharp resonance peak or *white line* related to

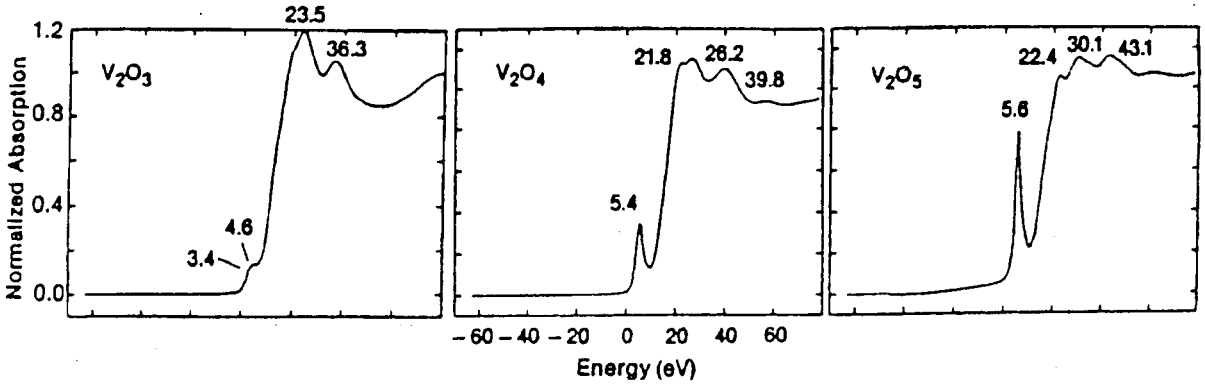

Figure 3. K edges in vanadium oxides; the site symmetry and the valence state of the resonant atom affect the XANES spectrum (prepeaks, energy shift of the absorption edge). (Reprinted with permission from ref 23. Copyright 1984 American Physical Society.)

transitions from a deep core level to energetically compact final states.[19] This strong resonance is generally larger for absorption edges occurring at low energies (L and M edges of transition or rare earth metals, for example). The edge resonance is sometimes so sharp that its observed width and intensity could be affected by an inadequate experimental resolution, a consideration that implies some requirements for the diffraction experiment itself. The minimum line width is determined by the natural level width of the core vacancy of the given absorption edge. It can vary from 0.30 eV for the Na K edge, 1.33 eV for the Co K edge, 5.31 eV for the Pt L_{III} edge, to 49.3 eV for the Pt K edge (tabulated or experimental values can be found in refs 20−22).[20−22]

(ii) An energy shift of the edge position occurs for different valence states, and at energies close to the edge (0−50 eV), the X-ray absorption near edge spectroscopy spectrum (XANES) of the same element may be very different, as shown experimentally for vanadium oxide by J. Wong et al.[23] (Figure 3). Furthermore as shown by theoretical calculations and by numerous XANES spectra,[24−26] $\mu_a(E)$ near edge absorption spectra and consequently variations of $f_a''(E)$ and $f_a'(E)$ are very sensitive to the geometric environment of the absorbing atom.

(iii) Due to this local environment sensitivity, for low local site symmetry of the absorbing atom, $\mu_a(E)$, $f_a''(E)$, and $f_a'(E)$ are polarization dependent.[27] Dichroism (spectral dependence with polarization states) can be observed in resonant diffraction data as it was observed for absorption. Thus, as for the absorption $\mu_a(E)$ and the index of refraction $n(E)$, the resonant scattering part, $f_a'(E) + if_a"(E)$, of the atomic form factor should be represented by a complex tensor rather than by a complex scalar number.[28−30]

(iv) Photons are sensitive to magnetization densities, and although for many years X-ray magnetic scattering was considered a curiosity, spectacular enhancements of this interaction occur near absorption edges due to resonant phenomena which exhibit a polarization dependence closely related to that occurring for charge scattering.[31,32]

(v) Extended oscillations, due to interference effects with neighbors, appear at energies above the edge (50−1000 eV) in absorption spectra (EXAFS); they affect resonant scattering factors and diffracted intensities in the same way.

The sensitivity of the resonant scattering factor to atomic chemical states and environments gives a small taste of the power of this method and also of its complexity. Consequently, from the beginning of any resonant diffraction analysis, the chemical sensitivity of resonant peak shape, position, and oscillations implies an experimental determination of $\mu_a(E)$, $f_a''(E)$, and $f_a'(E)$ on the same sample with the same experimental setup and the same energy resolution as that used for a resonant diffraction experiment.

III. Experimental Determination of Resonant Dispersion Factors

Resonant diffraction applications are based on the variation of the structure factor of Bragg reflections due to variations of f_a', f_a'' near the edge of one specific atom a, and several studies can be performed. If resonant atoms occupy different crystallographic positions or have different valence states, f_a', f_a'' can be extracted from diffracted intensities, allowing combined diffraction and spectroscopy analysis. On the other hand, if we know f_a' and f_a'', we can use the energy variation of resonant dispersion to extract structural information from resonant diffraction data. The accuracy of such an analysis is directly related to the quality of the experimental determination of f_a' and f_a''.

Theoretical determinations for the free atom[15−18,9] give the step-like shape at the edge and the smooth variation between edges but do not give edge features that are sensitive to chemical effects. Thus, an experimental determination of f_a' or f_a'' must be undertaken near edges on the sample itself. However, to apply the Kramers−Kronig relation, f_a' or f_a'' must be known in a very large energy range (from ∼30 eV to ∼200 keV for an absorption edge near 10 keV), and for such calculation, theoretical values are generally used far from the edge and merged to experimental values. As shown initially by Templeton et al.,[33] it is also possible to apply the Kramers−Kronig relation on the difference spectrum (experimental factor minus the theoretical one), the final resonant factor being the sum of the result and the tabulated theoretical factor.

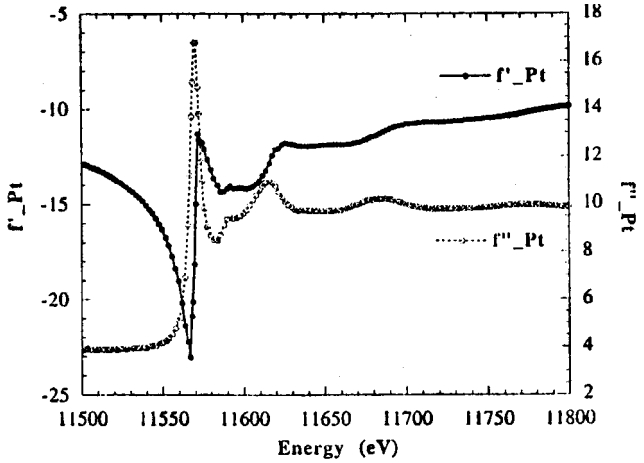

Figure 4. f' calculated using a Kramers−Kronig transform from the observed f'' spectrum extracted from absorption on platinum oxides and theoretical values calculated far from the Pt L_{III} edge. (Reprinted with permission from ref 34. Copyright 1997 Université Joseph Fourier, Grenoble.)

A. Direct Determination of f_a''

The absorption spectrum is directly related to f″: $\mu(E) = \sum_a (1/4\pi\epsilon_o)(2e^2/mc^2)\lambda\rho_a f_a''(\lambda)$ (ρ_a = number of atoms a per unit volume). Such measurements are relatively easy to obtain, even on nonstandard samples. They can be collected either in transmission mode or (especially for diffraction experiments) by measuring the fluorescence on the sample itself, in parallel with the resonant diffraction measurement. Owing to the high precision of this method, total EXAFS oscillations and chemical shifts can be measured on the sample itself and the total dispersive term $f'(E)$ can be obtained through the Kramers−Kronig relation (Figure 4).[33−35]

B. Direct Measurement of f_a'

Resonant scattering factors (mainly the f_a' term for powders and centrosymmetric structures) can be obtained from *intensity measurements of Bragg reflections* and refinements from a known single crystal or powder.[13,36,37] As shown in Figure 5, early dispersion factor measurements, obtained by this method, exhibited a sharp *white line* and some structures beyond the different L Cs edges.

The measurement of the real part $1 - \alpha(E)$ of the *refractive index* $n(E)$ is also a direct way of determining $f'(E)$. This can be performed by refraction of X-rays through a prism[38] or by total external reflection on a surface.[39,40] A total external reflection of photons occurs below a critical angle Θ_c. This critical angle is related to the refractive index of the reflected medium, and we can measure on the $f'(E)$ curve the same chemical shift as that observed in absorption. *Interferometry* is also a possible way of determining $f'(E)$, but this method is not easy to perform on ordinary sample.

Another way to measure this real dispersive factor is to use the small *angular shift* ($2d(n^2 - \cos^2\Theta)^{1/2} = k\lambda$) *of the diffracting angle* 2Θ relative to the Bragg angle ($2d \sin\Theta_B = k\lambda$). This shift is generally very weak, but it can be used to determine $f'(E)$ in an accurate way, as demonstrated in multilayers analysis.[41]

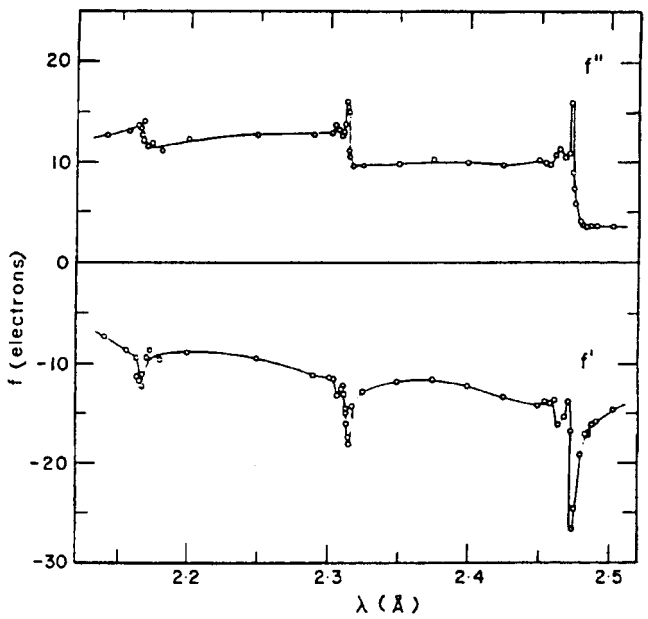

Figure 5. f', f'' of Cs, refined from the relative intensities of several reflections of $CsHC_4H_4O_6$ near the cesium L edges. (Reprinted with permission from ref 36. Copyright 1980 International Union of Crystallography−Munksgaard.)

C. Comparison of different f_a' and f_a'' Determinations

An early comparison between $f'(E)$ terms obtained on the same Cu compound by (i) X-ray absorption measurements and the Kramers−Kronig dispersion relation,[42] (ii) diffraction refinements of Bragg reflections from a single crystal,[37] and (iii) X-ray interferometry measurements near the Cu K edge[43] was already very satisfactory.[38] The differences are only <0.5 e$^-$; a discrepancy on the same order of magnitude also exists between experimental and theoretical curves. More recently, on the same sample and during the same diffraction experiment, simultaneous measurements of $f'(E)$ were reported from the 2Θ diffraction angle shift and $f''(E)$ from the diffracted reflection width, related to the absorption penetration length, and their corresponding Kramers−Kronig transformation.[41] The good agreement in this comparison (Figure 6) means that although the determination of $f''(E)$ from absorption data is easiest, $f'(E)$ determinations are also reliable at low energies.

IV. Resonant Scattering for Structure Factor Phase Solution (MAD Method)

During diffraction experiments, the measured intensities are proportional to the squared modulus of the structure factor $F(hkl)$. The phase information of this complex quantity is therefore lost, and the central problem for structure determination is to obtain the structure factor phases. Methods that are successful in small molecule crystallography (*heavy atom method, direct methods*) cannot be easily extended to large molecules. Thus, new methods have been developed, mainly in biological crystallography,

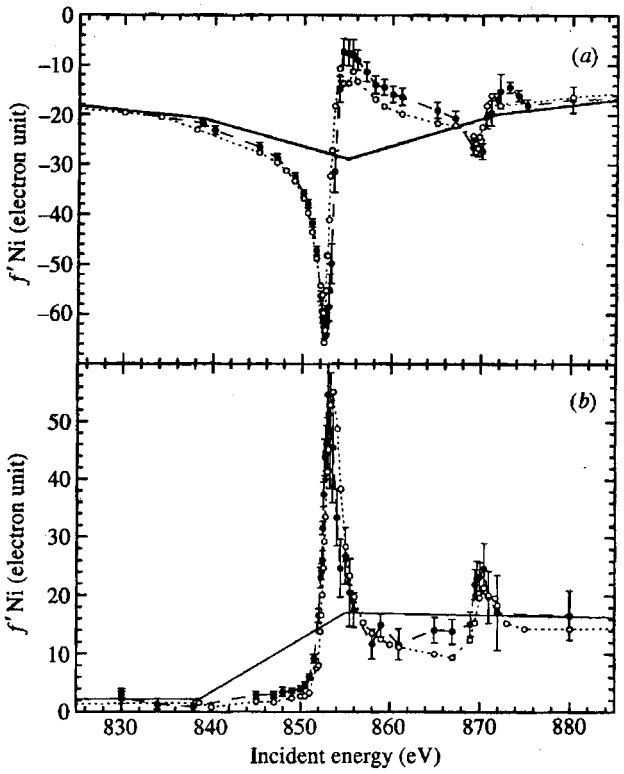

Figure 6. Comparison of f',f'' values extracted independently at the Ni L_{III} and L_{II} edges on an Ag/Ni multilayer from the analysis of the position (f' in part a) and width (f'' in part b) of the Bragg reflection (filled circles) and their Kramers−Kronig (a) and inverse Kramers−Kronig (b) transformation (open circles). Henke's theoretical values are also represented. (Reprinted with permission from ref 41. Copyright 1998 International Union of Crystallography−Munksgaard.)

to extract experimental phase information by varying the scattering power of an atom in the structure (isomorphous replacement with heavy atoms (MIR), multiwavelength anomalous diffraction (MAD)).[44−47]

A. Fundamentals of MAD Phase Evaluation

The complex structure factor can be represented geometrically as in Figure 7. In the absence of anomalous dispersion factors, the Friedel pairs F^+, F^- have the same modulus. The phase change, induced by the anomalous absorptive term f'' which has a $\pi/2$ phase shift with respect to f_o and f', gives rise to a change in their magnitude.

The difference between mates of a Friedel pair, which is used for the *absolute determination* of molecules, is one of basic principles of the MAD method. This method was first described 40 years ago for structures of crystals containing heavy atoms[48−50] and was nicely demonstrated in the 1980s for a protein structure determination by Hendrickson and Teeter.[51] The structure of crambin was solved at 1.5 Å resolution directly from the diffraction data of a native crystal, exploiting the small anomalous scattering of sulfur atoms at a single energy remote from the sulfur absorption edge ($E_{beam} \sim 9000$ eV, Cu Kα radiation, $f_S'' = 0.56$ e$^-$). Although this textbook example was performed on a classical X-ray source, the method is better suited using the energy-tunable radiation at synchrotron radiation facilities. These sources allow (i) an increase of the resonant scattering contribution by collecting diffraction data sets at energies close to an absorption edge of an atom of the sample and (ii) a variation of the resonant factors with X-ray photon energy to extract reflection phase information from its different intensities. For the MAD data analysis, a great improvement was introduced by Karle, who separated wavelength-dependent and wavelength-independent factors in an algebraic analysis of the structure factor equations.[52] This analysis allows energy-dependent parts of equations to be treated separately.[44] The representation developed here is that of Hendrickson, who separates F into nonanomalous contributions F_T and anomalous contributions $(F_A' + iF_A'')$[53]

$$F(H) = F(hkl) = |F| \exp(i\Phi) = (\sum_j f_{oj} e^{2\pi i(Hr_j)} e^{-T_j} + \sum_a f_{oa} e^{2\pi i(Hr_a)} e^{-T_a}) + \sum_a (f_a' + if_a'') e^{2\pi i(Hr_a)} e^{-T_a}$$

$$F(H) = (\sum_j (F_N)_j + \sum_a (F_A)_a) + \sum_a (F_A' + iF_A'')_a = F_T + F_A' + iF_A''$$

(nonresonant + resonant atoms)

with $F^+ = F(hkl)$, $F^- = F(-h-k-l)$, $F_T = |F_T| \exp(i\Phi_T)$, $F_A = |F_A| \exp(i\Phi_A)$, $\delta\Phi = \Phi_T - \Phi_A$.

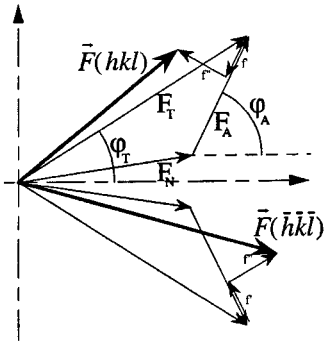

$F^+ = F(hkl)$ $F^- = F(-h-k-l)$
$F_T = |F_T| \exp(i\Phi_T)$
$F_N = |F_N| \exp(i\Phi_N)$
$F_A = |F_A| \exp(i\Phi_A)$
$F = F_N + F_A + F_A' + iF_A''$
$F = F_T + F_A' + iF_A''$
F_N : f_o scattering and smooth anomalous terms of normal atoms
F_A : f_o scattering of anomalous atoms
$F_A' + iF_A''$: contribution of anomalous scattering factors (f_a', f_a'') of anomalous atoms
F_T : non anomalous scattering f_o of all atoms $F_T = F_N + F_A$ (including those of the anomalous scatterer)

Figure 7. Effect of anomalous dispersion on a diffracted intensity (geometrical representation).

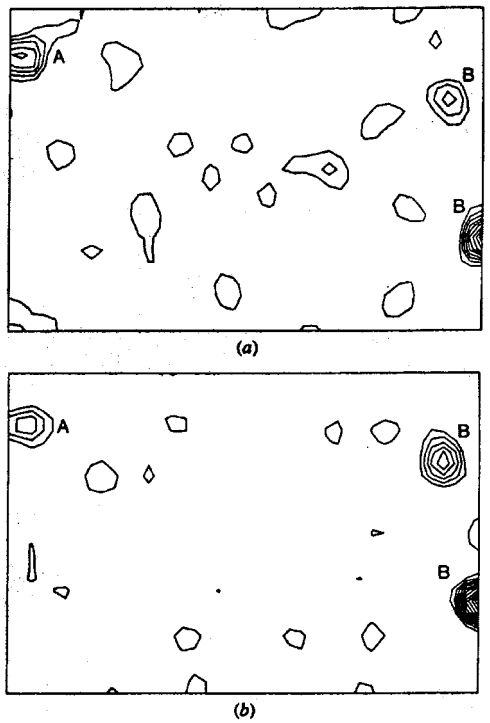

Figure 8. Bromine positions in a brominated oligonucleotide crystal as shown by a Patterson map calculated with (a) coefficients based upon anomalous or Bijvoet differences recorded at the *f″* maximum ($I^+ - I^-$) and (b) coefficients based upon dispersive differences between data sets collected at two energies ($I_{Ei} - I_{Ej}$). (Reprinted with permission from ref 56. Copyright 1996 International Union of Crystallography—Munksgaard.)

This leads to equations that contain three energy-independent parameters $|F_T|$, $|F_A|$, $\delta\Phi$. For a single type of anomalous scatterers

$$I^+ \alpha |F_T|^2 + ((f_a'^2 + f_a''^2)/f_{oa}^2)|F_A|^2 + 2(f_a'/f_{oa})|F_T||F_A|\cos(\delta\Phi) + 2(f_a''/f_{oa})|F_T||F_A| \sin(\delta\Phi)$$

$$I^- \alpha |F_T|^2 + ((f_a'^2 + f_a''^2)/f_{oa}^2)|F_A|^2 + 2(f_a'/f_{oa})|F_T||F_A| \cos(\delta\Phi) - 2(f_a''/f_{oa})|F_T||F_A| \sin(\delta\Phi)$$

From these equations, the f_a'' term shows up in the *Bijvoet (or anomalous) differences* ($I^+ - I^-$) which, at a given energy, are proportional to $f_a'' \sin(\Phi_T - \Phi_A)$. Several energy data are, however, needed to extract f_a'. *Dispersive differences* ($I_{Ei} - I_{Ej}$) depend mainly on ($f_{Ei}' - f_{Ej}'$) and $\cos(\Phi_T - \Phi_A)$. As f_a' and f_a'' are assumed to be known at each energy, $|F_T|$, $|F_A|$, and $\delta\Phi$ can be determined. Using these dispersive and Bijvoet differences as Fourier coefficients, it is possible to calculate dispersive and Bijvoet Patterson maps (Figure 8), which give the positions of the anomalous scatterers. From theses positions, the phase Φ_A of the anomalous scatterer can be calculated and thereby gives access to the phase Φ_T of the structure factor. This finally allows the electron density map to be calculated.[54−57]

B. Experimental Procedure and Applications

To get the best phasing power, energies must be carefully chosen to yield large values of $f_a''_{Ei}$ but also

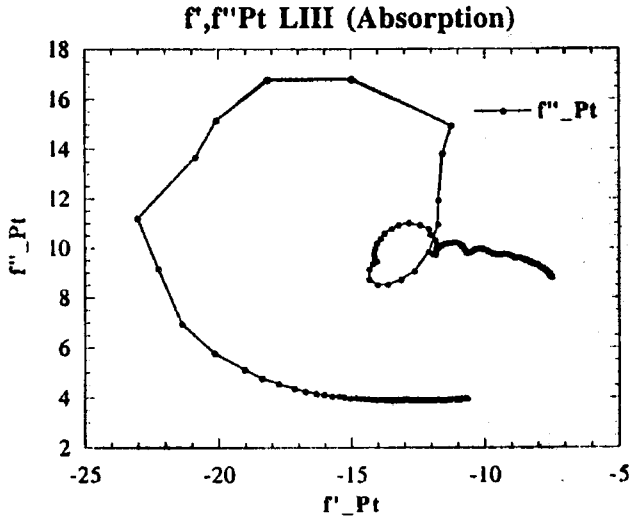

Figure 9. *f′/f″* loop corresponding to the *f′*(*E*) and *f″*(*E*) spectra of platinum oxide, near the Pt L_{III} edge, represented on Figure 4. The main loop corresponds to the "*white line*" at the edge; secondary loops correspond to EXAFS oscillations after the edge.

large differences ($f_a'_{Ei} - f_a'_{Ej}$). At least two energies close to an absorption edge should be chosen, one corresponding to the largest value of f_a'' (maximum of the *white line*) and one to the inflection point of absorption which corresponds to the largest modulus of f_a'. A third energy should be taken far from the edge to have strong differences in ($f_a'_{Ei} - f_a'_{Ej}$). In principle, only two energies are necessary so that the maximum variation of f_a' could be skipped. The best combination for energies that gives accurate phase determination for each reflection is directly related to the area of the loop described by f_a'/f_a'' in its complex representation (Figure 9). Owing to smearing of the f_a' curve, the area of the f_a/f_a'' loop decreases when data are collected with a lower energy resolution. For anomalous experiments, high-energy resolution is therefore necessary to obtain a f_a'/f_a'' loop that is sensitive to chemical features. These fine structures in f_a' and f_a'' induce secondary loops on the f_a'/f_a'' loop; accuracy in energy and in f_a'/f_a'' determination is also important to obtain reliable phases.

The factor which limited the first MAD experiments was that biological crystals are often highly sensitive to X-rays and tend to degrade rapidly under the intense synchrotron beam. Cryocooling techniques (flash freezing, etc,) allow much longer data collections on a given crystal. In the 1990s these methods extended the MAD method to less "*X-ray resistant*" crystals and was a key development in the widespread use of this technique. They include, in the first place, metalloproteins that naturally contain metal atoms suitable for resonant diffraction, such as Fe atoms in the metalloprotein lamprey hemoglobin.[53,58] If no suitable anomalous scatterer (heavy atoms) is present in the macromolecule, it can be inserted as an extrinsic label. Some protein or nucleic acid complexes contain light metal atoms that can also be substituted by heavier ones such as lanthanides.[54,59,60] The most commonly used extrinsic anomalous scatterers are currently heavy atoms,

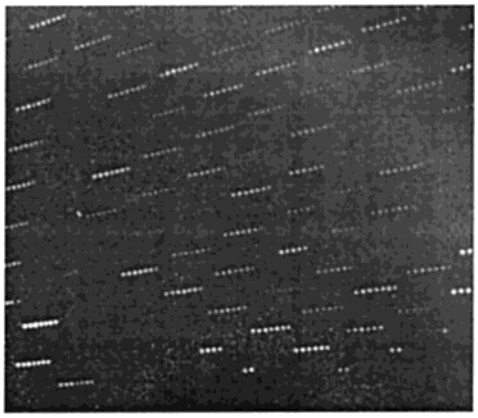

Figure 10. Simultaneous-MAD pattern collected in the dispersive diffraction experiment measured on a Cellulase A sample at the Hg L_{III} edge. The diffracted pattern displays for each reflection rows of seven peaks corresponding to seven energies. (Reprinted with permission from ref 65. Copyright 2000 International Union of Crystallography.)

lanthanides and selenium atoms, that can be substituted for natural sulfur in methionine.[61]

C. Further Developments and Prospects

Up to now, it was considered that it was better to improve the data accuracy at a few optimized energies (generally three) than to collect data at too many energies.[56,62] Nevertheless, with measurements at a large number of energies, the whole f_a'/f_a'' loop can be used for the phasing power and the phase error is reduced. The measurement of the intensity *gradient* of a reflection with respect to the energy also provides information on its phase free from the problem of intensity scaling.[63] As data collection from a large energy range is time-consuming, it was proposed to use energy dispersive optics to perform a *simultaneous-MAD* data collection[64,65] (Figure 10). Multiwavelength 2D-patterns must be analyzed by an ad hoc program to integrate reflections and normalize intensities[66] and to allow quantitative analysis. However, the higher background level of the dispersive method is an intrinsic limit related to the large number of wavelengths collected in parallel.

Another experimental development is based on the use of resonant scattering at soft X-ray energies to access the K edge of light atoms (Cl, S, P) and to obtain much stronger anomalous dispersion factors for heavy atoms. For example, at the U M_V edge ($E \sim 3545$ eV) there is a change of more than 100 e^- in the uranium scattering factor,[67,68] and similar variations occur at the L_{II}/L_{III} edges of the transition elements.[41] Figure 11 compares f_a'/f_a'' variations for uranyl M_V edge, lanthanide L_{III} edge, phosporus K edge, and selenium K edge.[69] This latter Se atom, which displays only 8 e^- at the f_{Se}'' maximum, is currently used as selenomethionine in proteins.[61] The gain in Bijvoet and dispersive differences is, respectively, proportional to f_a'' and f_a'; thus, the MAD phasing power would be highly efficient for the determination of large structures if difficulties related to the use of soft X-rays could be solved.[69]

MAD experimental developments are now being focused on undulator synchrotron beamlines with a

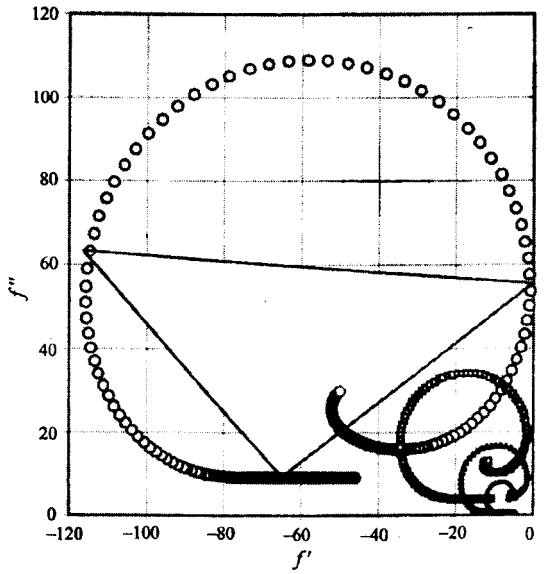

Figure 11. Comparison of anomalous dispersion f_a'/f_a'' (in electron units) of some elements at soft X-ray energies with those of selenium atoms (smallest loop). (i) (○) uranyl M_V edge ($E \sim 3545$ eV), (ii) (□) lanthanide L_{III} ($E \sim 5483$ eV), (iii) (△) phosphorus K edge ($E \sim 2143$ eV), and (iv) the smallest loop (—) selenium K edge ($E \sim 12658$ eV). The phasing power of the experiment is proportional to the area of the loop if a complete intensity versus energy spectrum is measured (for a three-energy experiment, the phasing power is proportional to the area of the drawn triangle). (Reprinted with permission from ref 69. Copyright 2000 International Union of Crystallography—Munksgaard.)

tunable-energy band-pass and monochromatic optics. The high intensity and small divergence of the undulator beam allow the study of smaller crystals and the measurement of higher resolution data. Nowadays, MAD is a well-established method in biocrystallography; consequently, on one hand, molecules are often designed for the application of resonant diffraction (e.g., incorporation of selenium for example) and, on the other hand, most synchrotron radiation facilities have developed several dedicated beam lines for MAD experiments.

It must be noted that resonant scattering has received much less attention for the solution of structures from the small molecule community. This is particularly true for single-crystal structures of small molecules, owing to the efficiency of conventional structure solution techniques (*direct methods*). This is also true for ab initio structural determination on powder, although a successful theoretical and experimental phasing demonstration was reported by Prandl.[70,71]

V. Element-Selective Diffraction (Contrast Method)

For X-ray diffraction, the ability to distinguish elements is related to the ratio of the number of electrons for each atom and the discrimination between element with close atomic numbers can be difficult. There are two different methods used to enhance this contrast. The first one uses resonant diffraction: around absorption edges, the atomic scattering factor variations range from 5 to 20 electron units (e.u.) per atom, thus providing an

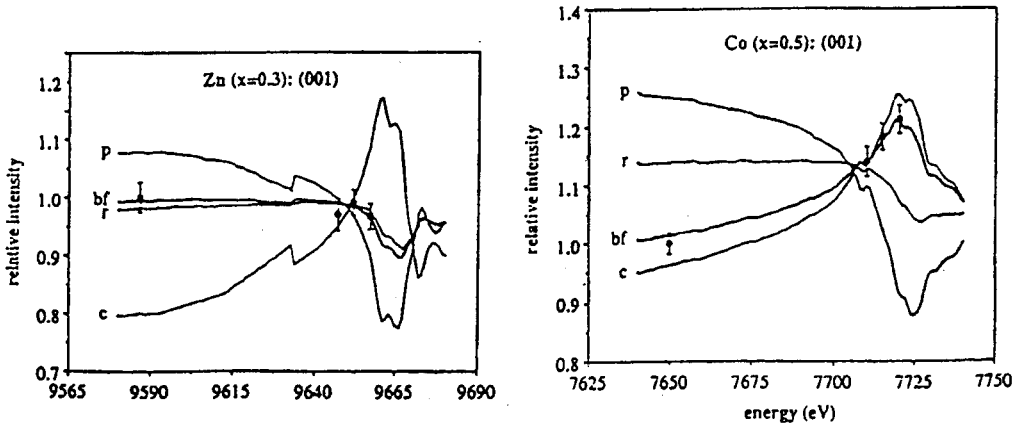

Figure 12. Intensity variation of (0 0 1) reflection for different localizations of Co and Zn in substituted $YBa_2(Cu_{3-x}M_x)O_7$ oxides. Experimental measurements at four energies for M = Co ($x = 0.5$) and Zn ($x = 0.3$), and calculated curves for (p) a plane site occupancy, (c) a chain site occupancy, (r) a random occupancy, and (bf) the best experimental fit. These spectra were used to prove that Co and Zn were randomly distributed on copper sites. (Reprinted with permission from ref 75. Copyright 1989 American Physical Society.)

additional contrast. The second method is obtained by neutron diffraction, since for neutrons the nuclear scattering length, which depends on the isotope and nuclear spin states, is not related to the atomic number. The efficiency of neutrons and resonant X-ray scattering for contrast studies has the same order of magnitude, so the use of the resonant diffraction method is based on the specificity of X-rays produced by synchrotron radiation relative to those of neutrons (sample size and absorption, sample environment, elements, and scattering factors/lengths, etc.). As the two techniques probe the same structural parameters through different particles (neutrons are scattered by nuclei and photons interact with electrons), the best accuracy for determination of element-selective parameters (occupancies, positions, temperature factors) is often obtained by joint refinement using both neutron and resonant X-ray scattering. However, resonant X-ray diffraction is an efficient technique which can be performed fully on a single (and small) sample.

A. Contrast between Neighboring Elements

One of the main uses of resonant dispersion in chemistry is to provide intensity contrast between neighboring elements in the periodic table. Thus, the determination of the distribution of the transition-metal or rare-earth atom, on the same crystallographic site is possible with X-rays.[72−74] This was shown by Howland et al.[75] on the high Tc superconductor $YBa_2Cu_{3-x}M_xO_{7-\delta}$, where the substitution of Cu by M = Fe, Co, Ni, and Zn has a drastic effect on the superconducting properties. X-ray-diffracted intensities at four energies close to the different K edges were collected and analyzed on a few sensitive reflections rather than full Rietveld refinements based on extended patterns (Figure 12). The analysis reported with a relatively good precision that for $x = 0.3$ Ni and Zn are randomly distributed on the two copper sites (planes and chains) while Fe and Co preferentially occupy Cu chains.[75] Such a contrast enhancement was also used for site occupancy analyses in spinel oxides,[76] for Zn-exchanged Na zeolite−Y,[77] and for high-pressure experiments to increase contrast between In and Sb at 3.5 GPa in a diamond anvil cell.[78]

The use of resonant scattering for contrast studies was also reported for single-crystal structure determinations.[79−82] Wulf[79] differentiates experimentally lead and bismuth ($Z_{Pb} = 82$, $Z_{Bi} = 83$) in the mineral structure of the galenobismutite $PbBi_2S_4$. For this analysis, the author uses the differential resonant δ-map which depends mainly of the variation of the real f' term and shows up only at the atomic positions of the resonant atoms.

On artificial samples such as multilayers where the number of reflections may be rather low owing to the poor epitaxy, resonant scattering increases the number of data sets of the same sample with different atomic contributions. This allows better density profile analysis of a specific element in superlattices.[83,84]

The complementarity of neutron and X-ray data was nicely demonstrated by Williams et al.[85] for transition-metal alloy with an ordered CsCl-type structure, where a simultaneous refinement determined the site occupancy of a very small addition (2%) of vanadium in the 50/48/2 Fe−Co−V compound. A comparative analysis of the contrast efficiency of resonant X-ray scattering relative to neutron diffraction was also reported by Warner et al.[86] They refined occupancies of the two sites possible for Co and/or Fe in $Co_2Fe(PO_4)_2$. In this compound, Fe and Co neutron scattering lengths are different ($b_{Fe} = 9.5\ 10^{-15}$ m, $b_{Co} = 2.5\ 10^{-15}$ m), and at 9 eV before the Fe K edge, the Fe resonant f' factor reaches a value close to −8 e.u., increasing the difference between Fe and Co scattering factors ($Z_{Fe} = 26$, $Z_{Co} = 27$). For both refinements the resulting Fe/Co occupancies are in agreement at the level of two estimated standard deviations (esds). These esds are nearly the same (1−2%) for the two radiations and confirm the equivalence of both techniques. It should be noted that for neutron data, scattering lengths can present large variations between elements and, in particular, the contrast can be tre-

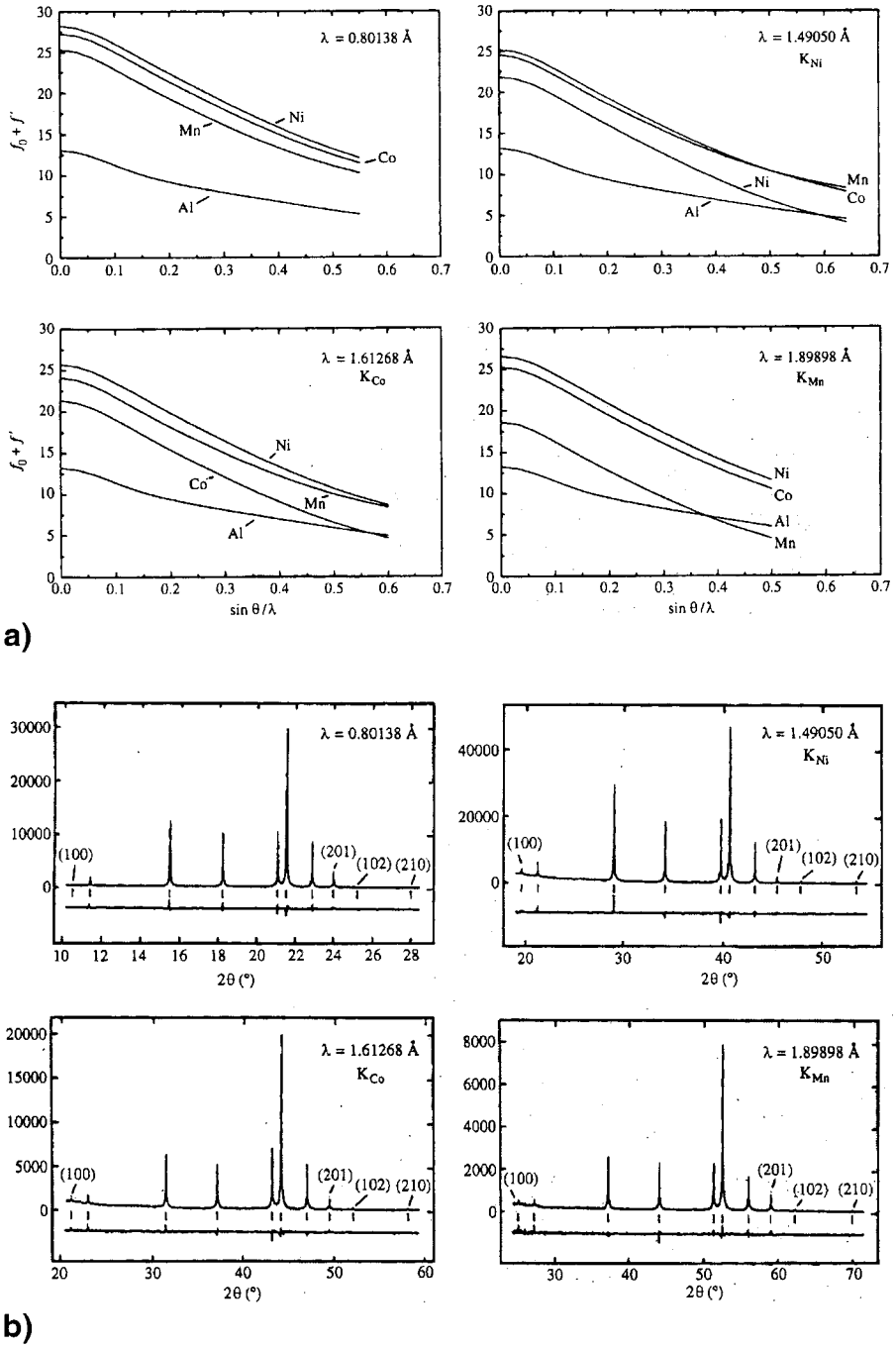

Figure 13. (a) Real scattering power ($f_o + f'$) of Ni, Co, Mn, and Al as a function of sin θ/λ for wavelengths or energies far and close to K edges of Ni, Co, and Mn atoms. (b) Low 2θ angle part of the observed and refined diffraction patterns of $LaNi_{3.55}Mn_{0.4}Al_{0.3}Co_{0.75}$ for the same wavelengths or energies. (Reprinted with permission from ref 92. Copyright 1998 International Union of Crystallography—Munksgaard.)

mendously improved for a compound with an atom having a negative neutron scattering length. This was demonstrated by Reimers et al.[87] in the intermetallic compound $(Mn_{1-x}Cr_x)Sb$, where the neutron scattering lengths are extremely different with a negative value for Mn ($Z_{Cr} = 24$, $b_{Cr} = 3.52\ 10^{-15}$ m; $Z_{Mn} = 25$, $b_{Mn} = -3.73\ 10^{-15}$ m).

B. Cation Localization in Complex-Substituted Samples

Another advantage of resonant diffraction is its ability to obtain diffraction patterns at the edges of several elements to solve complex substituted samples as shown in doped high-Tc superconductors or in ternary alloys.[88−93] An example of the importance of cation localization analyses is the study of the intermetallic compound $LaNi_5$ and its complex substituted derivatives[92,93] (Figure 13). These compounds have attracted important commercial interest because of their widespread application in rechargeable nickel metal hydride (NiMH) batteries to replace nickel−cadmium batteries because of their higher capacity and lower toxicity. Their electrochemical long-term cycling stability is improved by replacing part of Ni atoms by Mn and/or Co transition metals, and good properties are obtained for a multisubstituted sample

like $RE_1Ni_{3.55}Mn_{0.4}Al_{0.3}Co_{0.75}$.[92] Nevertheless, the role played by Co atoms is far from understood and there is a great interest to reduce this expensive element in NiMH batteries. Resonant scattering experiments at 20−10 eV before K absorption edges of Ni, Co, and Mn were performed to increase contrast between these elements with similar atomic numbers (Z_{Ni} = 28, Z_{Co} = 27, Z_{Mn} = 25). The variations of f' factors (∼ 5−6 e.u.) allow an inversion of scattering strengths of these atoms as shown in Figure 13a. Consequently, the intensity differences observed for the different patterns (Figure 13b) allow relatively small esds for atomic occupancy factors (∼0.01−0.03).[92]

One limitation of resonant contrast analysis is the correlation of temperature and scale factors with the resonant f' term. This problem may be minimized by performing experiments at wavelengths or energies at ∼10−20 eV before the absorption edge of the resonant atom: the variation of the f' term is still significant (−8 to −5 e.u. for transition metals), and we can use the theoretical f' and f″ values to avoid any correction due to the chemical state and the environment of the resonant atoms. It may also be minimized by measuring data from additional off-edge energy or by collecting a neutron diffraction pattern.

The complementarity of neutron data for contrast studies was used for the structure determination of the nonstoichiometric $La(Ni_{1-x}Cu_x)_{5+\delta}$ compound, which is derived from the same $LaNi_5$-type structure by the replacement of La atoms by Ni−Ni and/or Ni−Cu dumb bells.[93] For this sample, the resonant X-ray contrast is opposite to the neutron one: for data collected at an energy 14 eV before the Ni K edge, Z_{Ni} = 28, f'_{Ni} = −6.1 e.u., Z_{Cu} = 29, f'_{Cu} = −2.3 e.u., Z_{La} = 57, f'_{La} = −1.4 e.u. and b_{Ni} = 10.3 10^{-15} m, b_{Cu} = 7.72 10^{-15} m, b_{La} = 8.27 10^{-15} m.

Neutron and anomalous X-ray scattering were also collected for the analysis of high-Tc superconductors such as the thallium oxide since their compositions are uncertain due to the evaporation of thallium oxide at high temperature during the sample preparation. For example, Sinclair et al.[94] determined the composition and the cation distribution of the Tl2223 superconductor by using a combined refinement of one neutron, two anomalous X-ray data, and one off-edge pattern. For this complex and multiphase sample, they show that a substitution by Cu rather by Ca exists at the Tl sites, without vacancy formation.

As, contrary to neutron and resonant X-ray scattering, the Thomson normal scattering varies with $\sin\theta/\lambda$, neutron diffraction and resonant diffraction to some extent can also be used to improve the determination of Debye−Waller factors. A latter advantage of resonant dispersion is its ability to separate individual temperature factors and atomic coordinates when different species are mixed in the same site.[95]

C. Atomic Selectivity for Modulated Structure Analysis

For modulated structures, an analysis of the energy dependence of the intensity of satellite reflections gives specific information about displacements of a given atom.[96,97] For example, this can be used to study quasi-one-dimensional metals; these compounds exhibit Peierls transitions, where the material changes from a metallic to a semiconducting or isolating state, associated with a modulation of the metallic atoms. One puzzling example is $(TaSe_4)_2I$, which was recently analyzed.[98] This compound exhibits infinite ($TaSe_4$) chains, where Ta d_{z^2} overlaps create a 1D conducting band. From this one-dimensional character and from the fact that there is 0.25 electron per tantalum atom, one would expect a low-temperature Peierls transition and tetramerization of the Ta atoms, i.e., a modulation with vector q_m = (0 0 1). However, the analysis of the eight low-temperature incommensurate satellite reflections had failed to show this modulation in $(TaSe_4)_2I$, rather exhibiting an "*acoustic*" modulation, with a long modulation period and affecting all atoms. Resonant diffraction experiments around the Ta L_{III} edge was used to study specifically the modulation of the Ta atoms: this has shown, in fact, that satellite reflections with $l = 4n \pm 1.08$ exhibit a contribution from the Ta atoms whereas the corresponding satellite reflections with $l = 4n \pm 0.92$ do not have this contribution[99] (Figure 14). Since only (hkl) main reflections with $l = 4n$ have a contribution from the Ta atoms, this proves that there exists a modulation vector q_m for the Ta atoms with a component along c^* equal to 1.08, which corresponds to the expected Peierls modulation. In that case, resonant diffraction can separate the expected modulation of the metallic atoms from the dominant *acoustic* modulation.

D. Partial Structure Factor Analysis

Resonant scattering was used to study the diffuse scattering and to extract short-range pair correlation of atoms in crystalline solid solutions such as binary or ternary alloys.[100,101] This contrast enhancement can also be used for small angle scattering experiments to study compositional and topological inhomogeneities at the nano-/micrometer scale. Anomalous dispersion helps to separate the contributions of different particles, and this approach was used to study the solute partitioning during alloy decomposition.[102]

Differential anomalous scattering and partial structure factor analysis are efficient to study amorphous-like materials such as glasses, liquids, nanoparticles, and catalysts.[103−107] It can also be used for quantitative analysis of minority phases such as Pt metal inclusions on amorphous or crystalline substrates.[108,109]

Such analyses are highly sensitive to the concentration and position of the resonant atoms, and in the case of nanometer-sized zinc ferrite particles, it has been shown that an amorphous-like structure of zinc ferrite is present on their surface rather than a crystalline structure[104] (Figure 15).

VI. Diffraction Anomalous Fine Structure Data Analysis (DAFS Method)

The DAFS method combines in the same experiment X-ray diffraction and X-ray absorption fine

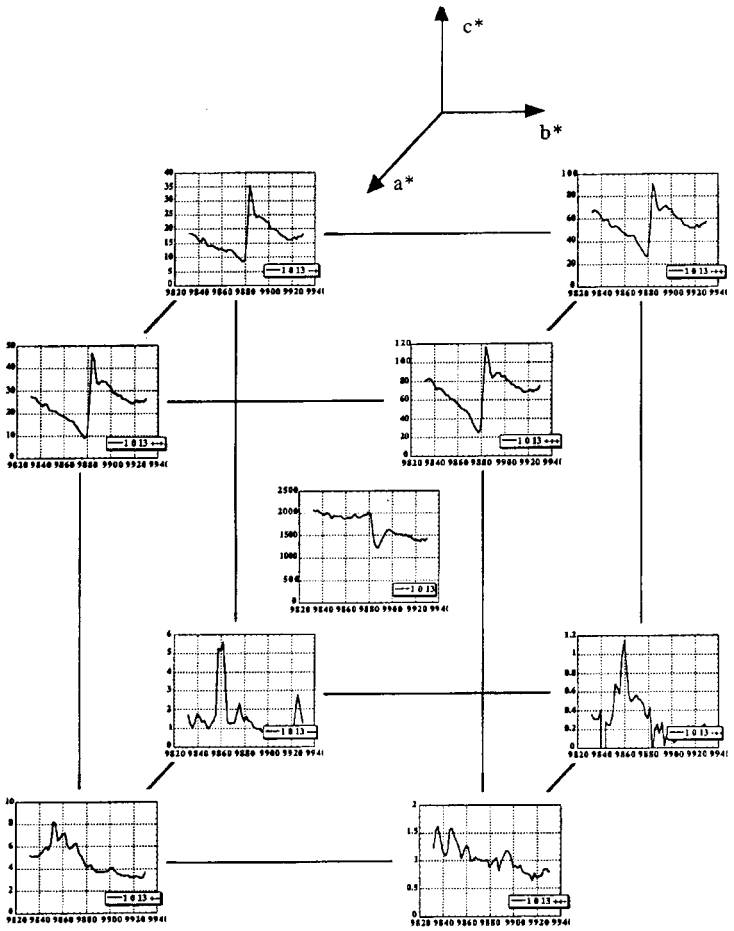

Figure 14. Resonant study of satellite reflections with l odd to search for tetramerization in $(TaSe_4)_2I$: satellite reflections are at $q = (\pm 0.05; \pm 0.05; \pm 0.08)$ for $T < 263$ K, resonant spectra corrected for absorption of (1 0 13) main reflection surrounded by its eight satellites: the resonant contribution that appears specifically for satellites with $l = 13 + 0.08$ (intensity ~ 100) and not for satellites with $l = 13 - 0.08$ (intensity < 10) is a signature of the modulated state of Ta atoms. (Reprinted with permission from ref 99. Copyright 1999 Université Joseph Fourier, Grenoble.)

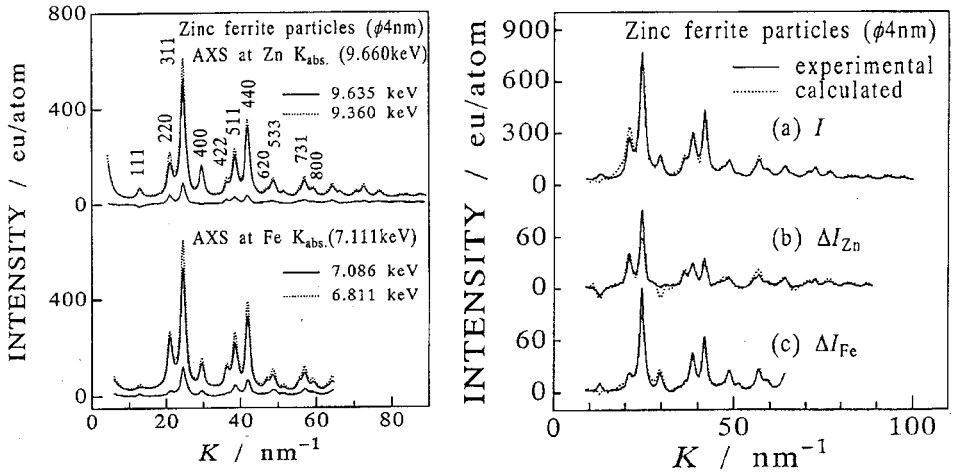

Figure 15. (a) Observed resonant X-ray scattering patterns of 4 nm zinc ferrite particles measured at two energies below the Zn and Fe K edges and the corresponding differential intensities. (b) Calculated patterns for the corresponding classical diffracted pattern and the two differential intensities obtained at the Zn and Fe K edges. The best fit is obtained for calculations (continuous lines) which substitute part of the scattering intensity of the crystalline particles by the scattering of amorphous $ZnFe_2O_{4-x}$ zinc ferrite. (Reprinted with permission from ref 104. Copyright 1994 Elsevier Science.)

structure (XAFS). In this way, the long-range structural information contained in diffraction peaks is combined with the chemical and local structure selectivity of X-ray absorption spectroscopy. Thus, it can provide *site-selective* and *chemical-selective* structural information. This combined technique offers the possibility of obtaining chemical information on mixed-valence oxides, phase-selective spectroscopy of mixed compounds, selective absorption spectra on multilayers, etc.

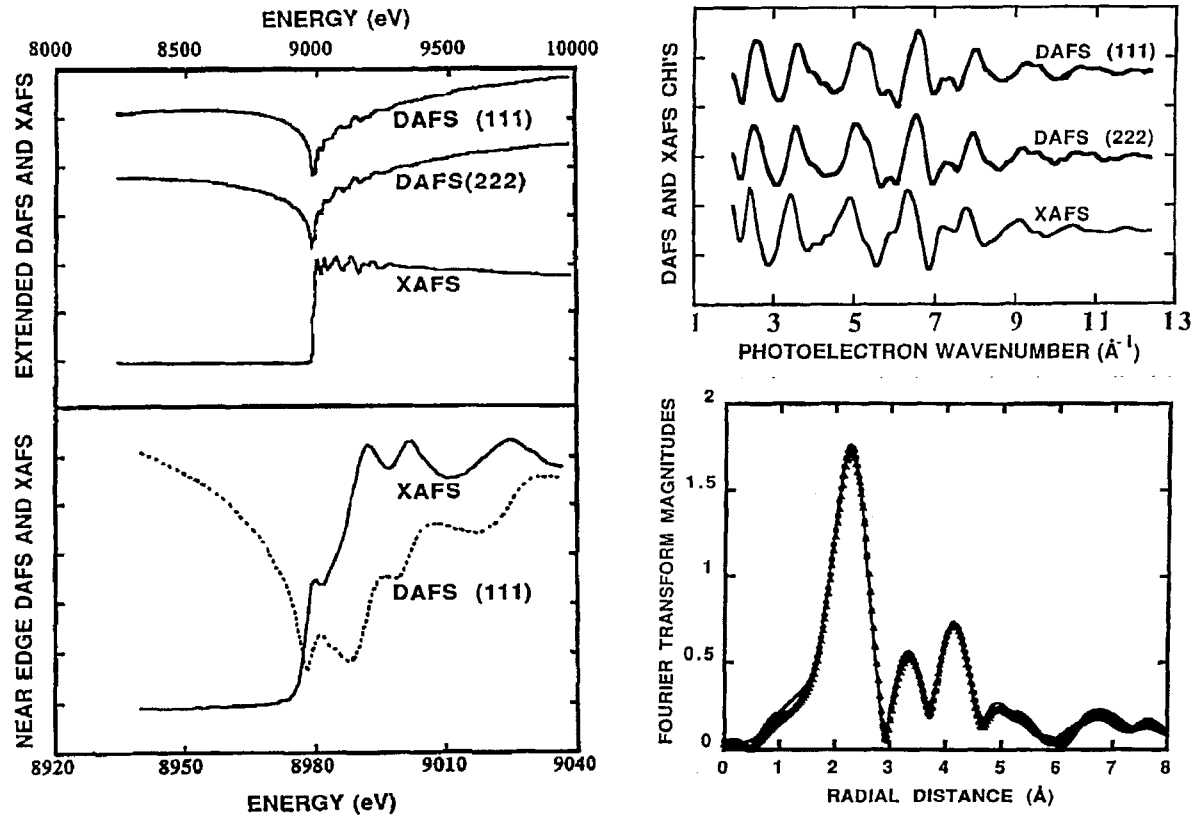

Figure 16. Comparison of the XAFS and DAFS spectra obtained on a Cu thick film at the Cu K edge. The same Fourier transforms are obtained from the different spectra. (Reprinted with permission from ref 114. Copyright 1992 American Physical Society.)

Although the first study of fine structure in X-ray diffraction was reported a long time ago,[6,110,111] almost no contributions developing this work were published during the 1960s and 1970s. It was with the development of synchrotron radiation sources in the 1980s that a few reports showed the feasibility of DAFS measurements[36,112,113] and in 1992 that Stragier et al.[114] and Pickering et al.[115] gave a demonstration of this method on a copper thick film and in powders, respectively. Later, several groups applied this method to different types of samples (thin films, multilayers, powders, single crystals).[116−124]

For atoms in solids, the scattering amplitude can be subdivided into smooth (free atom) and oscillating fine structure components $\chi_a(E)$. Such a separation of DAFS components is analogous to the standard XAFS separation of μ into smooth μ_o and oscillating χ_μ terms[116,124]

$$f_a(\Theta,E) = f_{oa}(\Theta) + f_a'(E) + if_a''(E) + \Delta f_a''(E)\chi_a(E)$$

$$\chi_a(E) = \chi_a'(E) + i\chi_a''(E)$$

As in the XAFS method, the site-selective distance information can be extracted from DAFS data. As shown in Figure 16, on a copper single crystal, only an absorption phase shift occurs between DAFS and XAFS spectra. XAFS provides atom-selective local information, and DAFS gives *atom- and site*-selective local information.

The aim of the DAFS analysis is to extract site-dependent f_a' and f_a'' curves from the diffraction intensity spectra measured as a function of energy. If the compound contains only one kind of anomalous scatterer *a*, the diffracted intensity can be written as follows:

(i) using the crystallographic formalism[14,53] by

$$I(E) = c_o[|F_T|^2 + ((f_a'^2 + f_a''^2)/f_{oa}^2)|F_A|^2 + 2(f_a'/f_{oa})|F_T||F_A| \cos(\delta\Phi) + 2(f_a''/f_{oa})|F_T||F_A| \sin(\delta\Phi)]$$

(ii) using the spectroscopic formalism[116,122] by

$$I(E) = c_o|F_T|^2 \cos^2(\delta\Phi)[1 + \gamma_s^2 + 2\beta_s f_a' + 2\gamma_s\beta_s f_a'' + \beta_s^2 (f_a'^2 + f_a''^2)]$$

with $\beta_s = |F_A|/(f_{oa}|F_T| \cos(\delta\Phi))$ and $\gamma_s = \tan(\delta\Phi)$[116]

$$\text{or } I(E) = c_o|F_T|^2[(\cos(\delta\Phi) + \beta f_a')^2 + (\sin(\delta\Phi) + \beta f_a'')^2]$$

with $\beta = |F_A|/(f_{oa}|F_T|)$.[122]

In all equations, $c_o = S\cdot LP\cdot A\cdot D/E^3$ where S is the scale factor, LP the Lorentz-polarization corrections, A the geometrical effect and the transmission coefficient due to absorption, and D a term corresponding to the detector efficiency and air path absorption; $|F_T|$, $|F_A|$, $\delta\Phi$, f_{oa}, f_a', and f_a'' are the same terms as defined above.

A. Data Analysis

The DAFS data analysis proceeds first by an *accurate energy calibration* of each intensity spec-

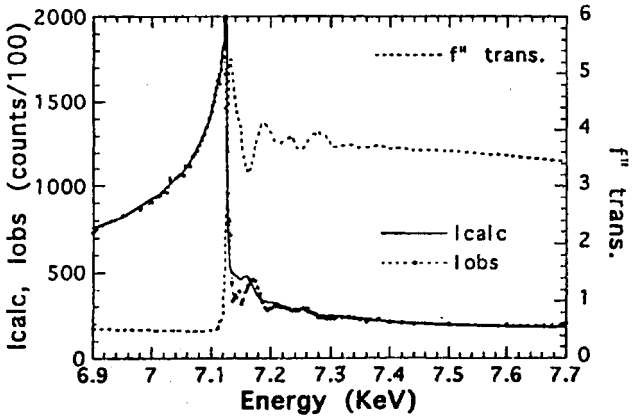

Figure 17. Intensity simulation of $BaZnFe_6O_{11}$ hexaferrite (0 0 33) reflection at the Fe K edge using theoretical free atom $f'(E)$ curves of Sasaki and only the measured absorption correction. (Reprinted with permission from ref 125. Copyright 1995 Elsevier Science.)

trum and an *accurate absorption correction* since the total absorption could be important for samples having a large anomalous scatterer content and could introduce intensity oscillations above the edge[125] (Figure 17). These oscillations are caused by the average absorption of all anomalous atoms *a* present on all sites of the structure. Removing these oscillations is vital for the DAFS analysis, since they represent "*average*" information, while we want to separate anomalous terms from different crystallographic sites: the diffraction process is site-selective but not absorption. For this, the absorption correction μ must be measured on the sample itself to take into account the chemical features of the sample.

Then, the calculation of site-selective f_a' and f_a'' curves can then be performed by using the energy dependent $f'_{(hkl)}$ and $f''_{(hkl)}$ values for each individual reflection (*hkl*) and later, from their different site contributions, the determination of the site-selective f_a' and f_a'' curves. This spectroscopic procedure was initiated successfully by Stragier et al.,[114] and it is the most convenient one for samples where the site-selective information can be directly extracted from selective reflections. This direct procedure of site-selective f_a' and f_a'' determination (and then that of χ_a' and χ_a'') was used for multilayers and thin films to separate their information from the buffer.[116,121,126] For example, DAFS experiments performed at both Ga and As K edges can extract GaAs distances in a buried $Ga_{1-x}In_xAs$ layer grown coherently on GaAs-(0 0 1).[122,123] From the diffracted spectra, high-quality *k*-weighted fine structures can be obtained (Figure 18), giving results in excellent agreement with XAFS spectra and models for strained-layer semiconductors. In relaxor ferroelectric $PbMg_{1/3}Nb_{2/3}O_3$, using superlattice reflection originating from ordered nanodomains, DAFS analysis can directly provide selective information of the local Nb atom in the domains.[127] This procedure was also used on samples like the Co_3O_4 spinel compound, whose space group gives rise to extinction rules and where, consequently, reflections exist for which only resonant scatterers located in one site could contribute[115] (Figure 19). On the high-Tc superconductor $YBa_2Cu_3O_7$, it was used to separate the individual f_a'' curves of the two copper sites.[116]

Another process for obtaining the site-selective f_a' and f_a'' spectra uses a simultaneous refinement procedure of several reflections at all energies. This method is convenient for samples where there are no reflections with a single contribution from only one site and was generally used by crystallographers on powders or single crystals.[74,89,90,128−131] It has been used for twinned single-crystal analysis of platinum oxide[132] and to separate Fe site contributions in hexaferrite $BaZnFe_6O_{11}$.[125] The structure of this latter compound contains four octahedral sites occupied by Fe cations and two tetrahedral sites occupied by Fe

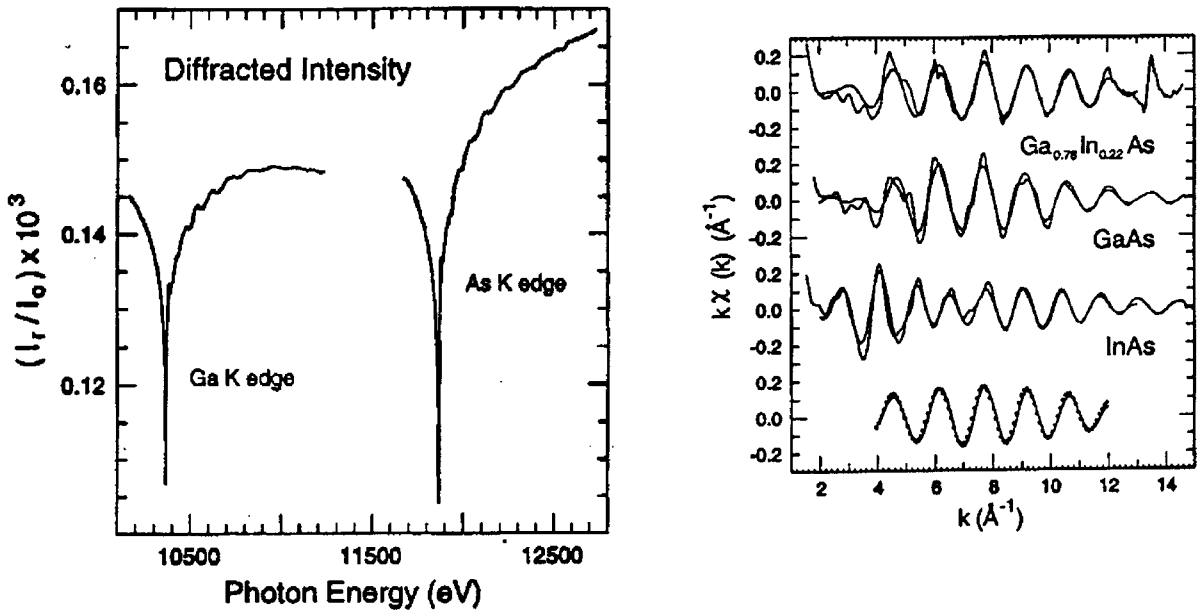

Figure 18. DAFS spectra of the (0 0 4) strained-layer reflection around the Ga and As edges on a $Ga_{0.785}In_{0.215}As$ layer grown on GaAs(0 0 1); corresponding *k*-weighted fine structure at the As K edge that gives the first- and second-neighbor distances around As atoms. (Reprinted with permission from ref 123. Copyright 1998 American Physical Society.)

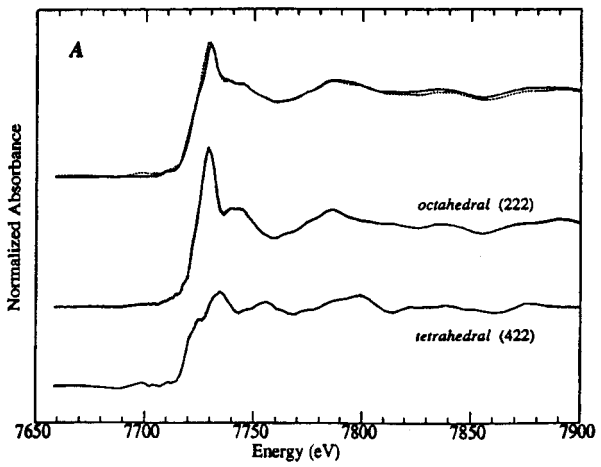

Figure 19. Cobalt near edge XAFS and DAFS spectra of Co_3O_4. The bottom curves show both spectra of the octahedral and tetrahedral cobalt site, directly extracted from the (2 2 2) and (4 2 2) reflections. The top curve compares the weighted sum DAFS spectrum with the XAFS one obtained from total absorption. (Reprinted with permission from ref 115. Copyright 1993 American Chemical Society.)

and Zn atoms. DAFS measurements of nine (0 0 l) reflections were performed to distinguish Fe cation contributions from tetrahedral and octahedral sites. First, the simultaneous refinement procedure of several reflections at all energies was performed far from the edge, using the measured transmission absorption coefficient, the theoretical f_a' and f_a'' curves, and intensity variations versus the energy are refined to determine all instrumental and samples parameters such as the atomic occupancies. Then the f_a' factors of the different sites are refined and f_a'' are calculated using the Kramers−Kronig relation (Figure 20). As shown in this figure, for strong reflections such as (0 0 33), oscillations are caused mainly by variations of the total absorption. In contrast, weak reflections such as (0 0 24), less sensitive to absorption, exhibit large DAFS oscillations; they could present a large phase change at the edge due to the small $|F_T|/|F_A|$ ratio, giving rise to an inversion of the intensity variation near the edge.

B. Valence Determination

As the DAFS methods presents a spectroscopic-like sensitivity, it can be used for valence studies in mixed-valence compounds such as the high-Tc superconductor $YBa_2Cu_3O_7$. If we study at a few energies for such a compound in which a single element could have different oxidation states at different sites, refinements of $f_a'(E)$, $f_a''(E)$ values can allow determination of the absorption chemical shift observed for the different sites[74,129−131] (Figure 21). However, the accuracy of such earlier determinations was limited by the small number of energies used.

Full spectra obtained by diffraction anomalous near edge spectroscopy experiments (DANES) give information on the valence state of the resonant atom with the same sensitivity as for X-ray absorption near edge spectroscopy experiments (XANES). Such experiments give very good results on thin films, and the site selectivity of DANES was nicely demonstrated on thin films of the high-Tc superconductor $YBa_2Cu_3O_7$ where Cross et al.[133] extracted the individual f_a'' curves of the two copper sites by using a corefinement of different reflections (Figure 22).

Such an analysis can be useful in solid-state chemistry. However, samples are often only available in a powder form and there are some intrinsic limits of the DANES method when applied to powders (low count rate, low f'' sensitivity, sampling problems, and fluorescence scattering).[74,115,129,134−136] For example,

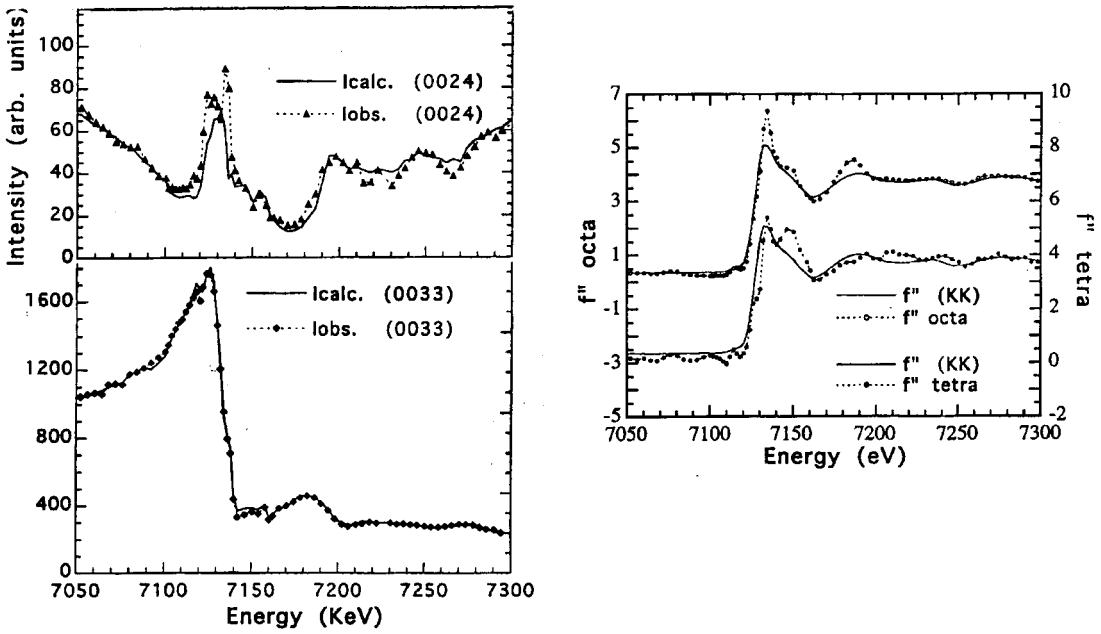

Figure 20. (a) DAFS spectra of the $BaZnFe_6O_{11}$ hexaferrite (0 0 24) and (0 0 33) reflections and intensity fits using bulk $\mu(E)$, refined individual $f_a'(E)$ and $f_a''(E)$ curves for tetrahedral and octahedral sites. (b) Corresponding $f''_{tetra}(E)$ and $f''_{octa}(E)$ hexaferrite spectra for the tetrahedral and octahedral sites derived from DAFS refinements and the Kramers−Kronig relation, the average $f''_{(KK)}$ spectrum being obtained from transmission XAFS experiments. (Reprinted with permission from ref 120. Copyright 1996 OPA Gordon & Breach Publishing.)

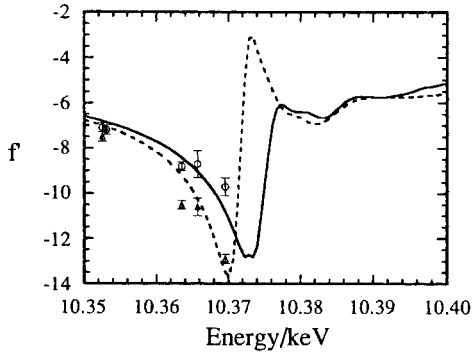

Figure 21. $f'(E)$ for Ga atoms in $GaCl_2$ near the Ga K edge, refined from anomalous powder diffraction. The triangles and circles are individually refined values for Ga^+ and Ga^{3+} sites, respectively; for comparison, $f'(E)$ curves obtained from reference absorption spectra are reported for Ga^+ (- - -) and Ga^{3+} (—). (Reprinted with permission from ref 129. Copyright 1992 International Union of Crystallography—Munksgaard.)

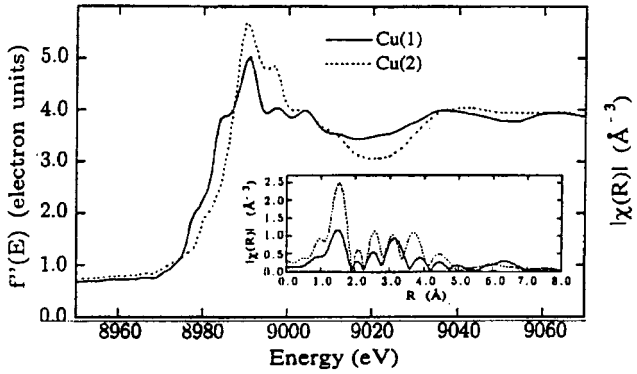

Figure 22. Site-separated $f_a''(E)$ spectra of the Cu1 and Cu2 atoms, extracted from a DAFS analysis on $YBa_2Cu_3O_7$ thin film; the inset shows the *R*-space transforms of the corresponding $\chi(Q)$ data that indicate the distances and numbers of first and second neighbors for each atom. (Reprinted with permission from ref 133. Copyright 1997 Editions de Physique Sciences.)

experiments were performed, at low energy near the Mn K edge, on a highly absorbing powder $La_4Mn_5Si_4O_{22}$ where there is no pure site-selective reflection (no systematic extinction for the resonant atomic site as it is for all spinel oxides). This compound is believed to contain three valence states of manganese (Mn^{4+}, Mn^{3+}, and Mn^{2+}), distributed over three crystallographic sites. Regarding data collection strategy, energy scans at fixed *Q* positions of selected reflections were preferred to the collection of complete powder patterns at 20−30 discrete energies. With an adequate sample spinning and a large acceptance analyzer (for a better sampling), good spectra of different diffracted intensities have been obtained as a function of energy. DANES analysis used a co-refinement of eight reflections containing crossed combinations of the three manganese sites.[135] The three different manganese sites of this powder display three different edge positions, each shifted relative to the other by 3 and 4 eV (Figure 23). Valence states and DANES studies can thus be performed on samples such as powders even if they are extremely absorbing. The statistics, however, is poorer than for single crystals, and the extended part of the spectra (EDAFS) cannot be extracted with accuracy.

C. EDAFS Determination

In contrast to the case of powders, accurate extended-DAFS spectra can be collected on epitaxial thin films or multilayers.[117,121−123] Most experiments have been undertaken to separate the different atomic local structures in the different layers, which is not possible using absorption spectroscopy since the contributions of all equivalent atoms in the different parts of the material are averaged. For example, it has been shown in Fe/Ir multilayers with thick Fe layers that, using $\chi(E)$ curves of several superstructure reflections (Figure 24), it is possible to probe selectively Fe atoms at the Fe−Ir interfaces (i.e., 6% of the total amount of Fe in the cell). The co-refinement of several superlattice reflections, measured at the Fe K edge, has allowed the extraction

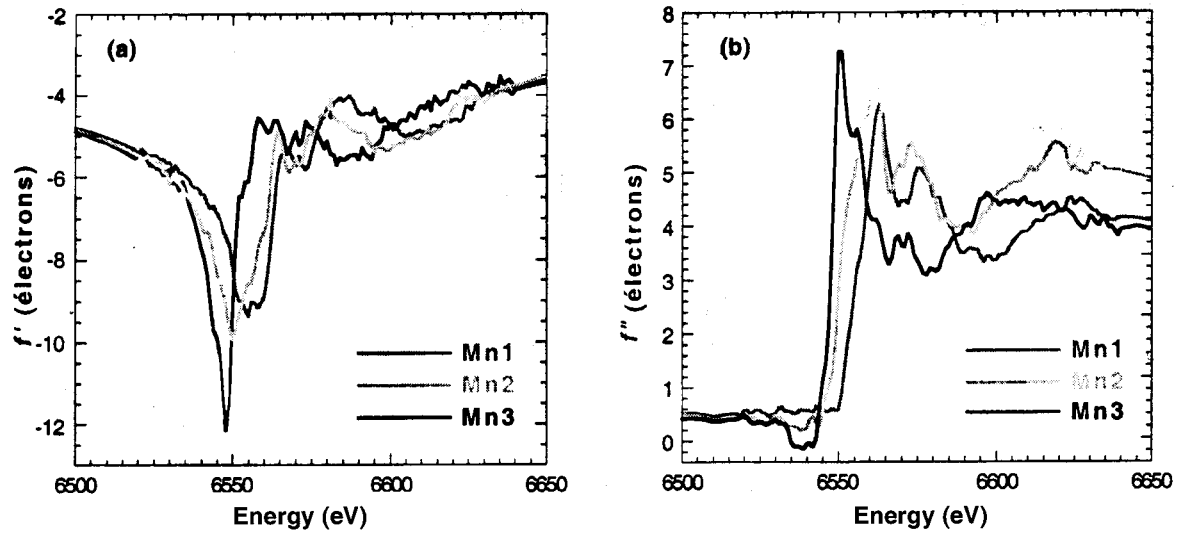

Figure 23. Energy shifts of the three site-selective $f'(E)$,$f''(E)$ spectra of the Mn1, Mn2, and Mn3 atoms, extracted by DANES analysis of a highly absorbing powder $La_4Mn_5Si_4O_{22}$. Each XANES spectrum is characteristic of the environment of the atom in its site and can be used to determine its valence and the site symmetry. (Reprinted with permission from ref 135. Copyright 1998 European Physical Society.)

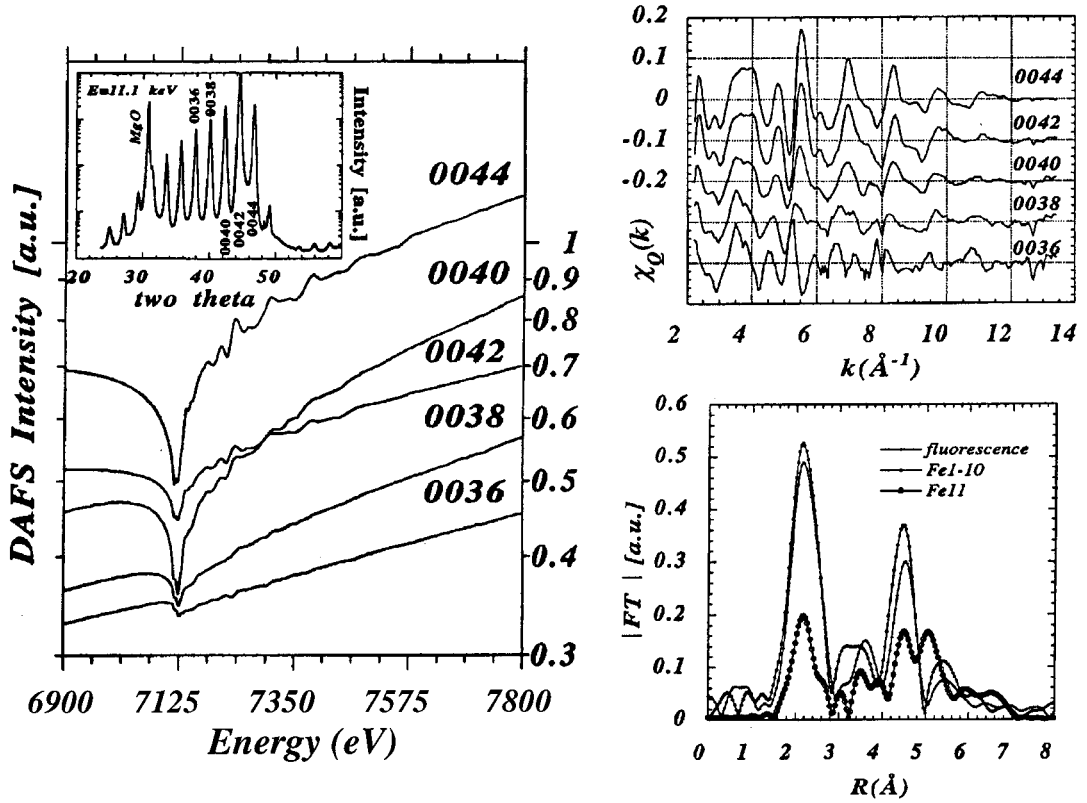

Figure 24. Raw DAFS spectra obtained from Ir/Fe multilayer Bragg reflections at the Fe K edge. Normalized EDAFS oscillation spectra for (0 0 36) to (0 0 44) reflections. Fourier transforms for the Ir-rich layers (Fe11), the Fe-rich layers (Fe1−11), and that extracted from fluorescence EXAFS data. These data have been used to differentiate first-neighbor distances for Fe atoms located in the middle and on the interface of the Fe layer. (Reprinted with permission from ref 117. Copyright 1997 American Physical Society.)

of oscillating $\chi(E)$ curves for Fe atoms localized either at the Fe middle layers or at the Fe−Ir interfaces. Their respective Fourier transforms gave first- and second-neighbor distances around the corresponding Fe atoms.[117] EDAFS spectroscopy can also be used to separate $\chi(E)$ oscillations of different X-ray absorption edges when two or more absorption edges are too close in energy in a given material, such as for the Ti K and Ba L edges in $BaTiO_3$.[124]

VII. Anisotropy of Anomalous Scattering

Using polarized X-rays provided by synchrotron sources, DANES spectra near absorption edges, such as XANES spectra,[26] can depend on the orientation of the local chemical environment of the resonant scatterer with respect to the beam polarization direction. This occurs when the resonant atom presents a coordination with a low symmetry like the uranyl ion in the salt $RbUO_2(NO_3)_3$ or the Pt^{2+} cation in K_2PtCl_4.[28,137] This dichroism is observed most easily if the compound contains a single orientation for the site of the resonant ion. For example, in the salt $RbUO_2(NO_3)_3$, the linear O−U−O ions lie on the 3-fold axes of the rhombohedral crystal and an edge shift of ∼2 eV can be clearly seen in the absorption curve for polarized X-rays near the U L_{III} edge (Figure 25a). Due to the anisotropic anomalous scattering (AAS), this dichroism can be observed on more symmetric crystals such as in the $P2_13$ cubic $NaUO_2(C_2H_3O_2)_3$ compound in which each uranyl ion lies on a 3-fold axis and the difference patterns $f_\sigma'' - f_\pi''$ and $f_\sigma' - f_\pi'$, extracted from diffracted intensities at the U L_{III} edge, clearly agree with the curves obtained from polarized absorption experiments on the rubidium uranyl salt[28] (Figure 25b).

The site selectivity of DANES spectra can be used to separate the polarization dependence of dispersive terms for cations with different coordination environments and distinct oxidation states. For example, in the $Cs_2Au_2Cl_6$ compound, the f' and f'' dispersive terms are largely different for the Au^+ and Au^{3+} sites and the Au^{3+} cations give rise to a highly anisotropic scattering contribution at the Au L_{III} edge.[138] This anisotropic anomalous scattering is highly sensitive to the energy resolution of the scattering experiments: the maximum variation of the scattering amplitude with respect to the polarization direction can increase from 1 to 8 e.u. by improving the energy resolution from 10 to 1 eV.[139]

Thus, for resonant scattering experiments performed with a good energy resolution on compounds with resonant atoms in low-symmetry sites, the anomalous scattering factor must be replaced by a tensor to take into account polarization of both incident and diffracted beams. This effect is a sophistication of resonant effects, but it is also a new means of solving problems. Novel applications make use of this cross-term contribution $\sigma\pi$ of the resonant tensors, to which dichroic atoms contribute.[30] The scattering of the dichroic atoms can be easily ob-

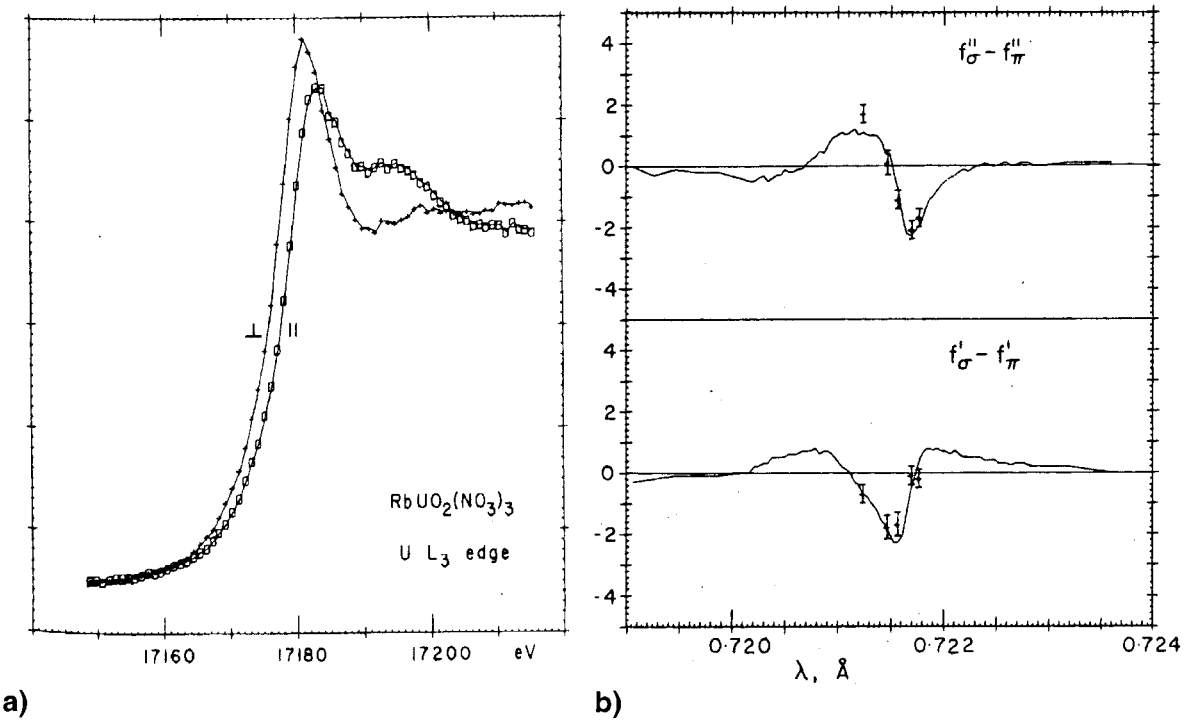

Figure 25. (a) Absorption curves near the U L_{III} edge in $RbUO_2(NO_3)_3$ for polarized X-rays with an electric vector parallel and perpendicular to the uranyl axis. (b) Polarized anisotropy of f' and f'' dispersive terms for the uranyl ion near the U L_{III} edge, represented by the difference patterns $f_\sigma'' - f_\pi''$ and $f_\sigma' - f_\pi'$. Points with error bars are determined from diffraction experiments on $NaUO_2(C_2H_3O_2)_3$, and continuous curves are obtained from the absorption measurements on the rubidium salt (a). (Reprinted with permission from ref 28. Copyright 1982 International Union of Crystallography—Munksgaard.)

served, independently of the surrounding structure, by using a polarization-selective detector.

Anisotropic anomalous scattering is almost averaged out in disordered samples and in powders. However, it can be extracted by the DAFS method, even in powders.[115] In anisotropic crystals, AAS can be easily observed. It explains the observation of reflections that are forbidden by a screw axis or glide plane, and their intensity changes with the azimuthal angle.[140,141] Such an effect can be used for a partial structure analysis[142,143] or for an electronic environment analysis of distorted sites.[144−146] As point defects and atomic thermal vibrations decrease the symmetry of the local atomic environment, they can contribute to additional anisotropy of the resonant scattering and to forbidden reflections near absorption edges.[147] These forbidden reflections can also be used to probe the splitting and ordering of the unoccupied *p* and *d* densities of state for dipole and quadrupole transitions[148] and for orbital ordering studies in V_2O_3.[149] Several anisotropic factors, such as the anisotropy of the local atomic environment, magnetic ordering, and orbital ordering, can exist simultaneously in a crystal, and phenomenological expressions were developed to describe the scattering tensor in such cases.[150]

Resonant diffraction was recently used to investigate electronic fluctuations of the octahedral iron atoms in magnetite, which is considered to be the prototype for charge localization.[151,152] Near edge DAFS spectra of (0 0 2) and (0 0 6) forbidden reflections were reported, above and below the Verwey transition as a function of energy, versus crystal azimuthal angle and for different polarization ($\sigma\sigma$ or $\sigma\sigma + \sigma\pi$) of the scattering process (Figure 26). Their intensity analysis indicates *p*-orbital ordering for the octahedral iron atoms and *d*-orbital ordering for the tetrahedral ones. Furthermore, their appearance implies that all octahedral sites are structurally and

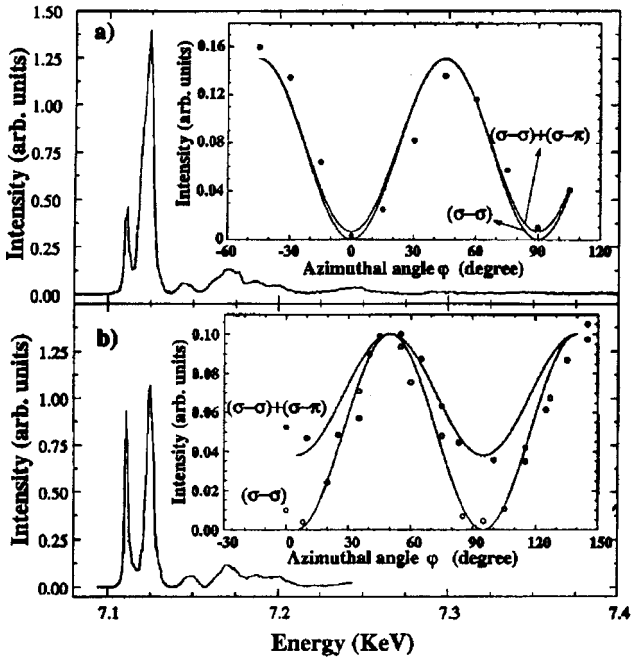

Figure 26. (a) (0 0 2) and (b) (0 0 6) forbidden reflections measured at the Fe K edge in magnetite at 300 K. The insets show the dependence of the integrated intensity at 7.124 keV as a function of the crystal azimuthal angle. (Reprinted with permission from ref 152. Copyright 2000 American Physical Society.)

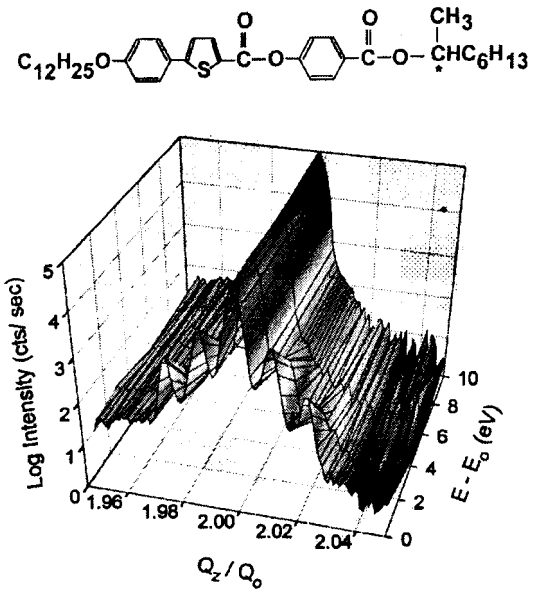

Figure 27. X-ray intensity in the Sm−C* phase of the MHDDOPTCOB as a function of Q and energy, near the sulfur K edge. Shown on top is the MHDDOPTCOB molecular structure. (Reprinted with permission from ref 154. Copyright 1999 American Physical Society.)

electronically equivalent down to a time scale shorter than the interaction time of the resonant virtual process involved.

Another application of the tensor nature of the dispersion factors is their use for the structural characterization of chiral mesophases.[153,154] Several chiral smectic-C variants were found in liquid crystal compounds, but previously, it has been impossible to obtain a detailed information about their molecular orientation. Resonant diffraction experiment performed at the sulfur K edge provided the direct structural evidence of several periodicities of the different Sm−C* phases. Due to the off-diagonal tensor components of dispersion, the scattered X-ray intensity varies depending on the relative orientation of molecules with respect to the polarization of the X-ray beam.[155] At the sulfur K edge only, this interaction generates superlattice diffraction peaks related to periodicity of the helical molecular arrangement[154] (Figure 27).

This anisotropy of the resonant dispersion factor can be introduced in Bragg intensity calculations by using components of the f_a', f_a'' tensors in the refinement of intensity as a function of energy.[156] For experiments with an energy resolution better than 10 eV, such anisotropy effects can be quantified, for example, for selenium in selenomethionine. Nevertheless, up to now, this effect was generally judged to be too small to be routinely introduced into MAD calculations, but a recent contribution shows that this variation can be used to help the determination of structure factor phases in the same way as changes of f_a' f_a'' with wavelength are used.[157]

VIII. Magnetic Resonant Scattering

The use of X-rays for the investigation of magnetism in matter is relatively recent. A theoretical prediction[158] and the first magnetic diffraction experiment, using conventional X-ray sources, were published in the 1970s.[159] Due to the smallness of the effect, magnetic scattering was considered to be a curiosity for a long time. However, since the development of synchrotron radiation sources, a large variety of experiments have been performed. Through its polarization dependence, nonresonant magnetic diffraction allows one to separate the orbital and the spin parts of the magnetic form factor. It has been shown theoretically and experimentally that strong enhancement of magnetic intensity occurs when the energy is close to an absorption edge of magnetic atoms.[160−162] This resonant intensity increase is particularly large near the M absorption edges of actinides[163] (Figure 28). The enhancement of the magnetic diffraction signal and the existence of magnetic dichroism arise from the same mechanism, which has been analyzed in terms of electric multipole transitions, whereas the purely nonresonant magnetic X-ray scattering originates from magnetic couplings.[31,164]

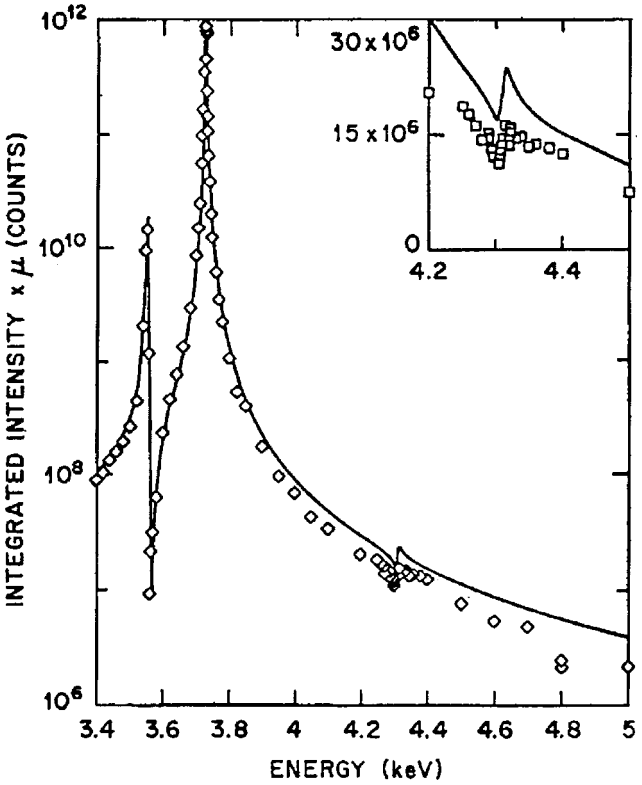

Figure 28. Energy dependence of the (0 0 5/2) magnetic reflection intensity, corrected for absorption, at the uranium M edges in UAs. (Reprinted with permission from ref 163. Copyright 1990 American Physical Society.)

Contrary to X-ray magnetic circular dichroism, which is sensitive only to the imaginary part of the resonant scattering amplitude, resonant X-ray magnetic scattering measures the square of the modulus of the total scattering amplitude including both the real part and the imaginary parts of the resonant scattering. Magnetic resonant scattering gives an element-selective information that can probe electronic structure and magnetic properties. Its sensitivity allows weak magnetic moments to be investi-

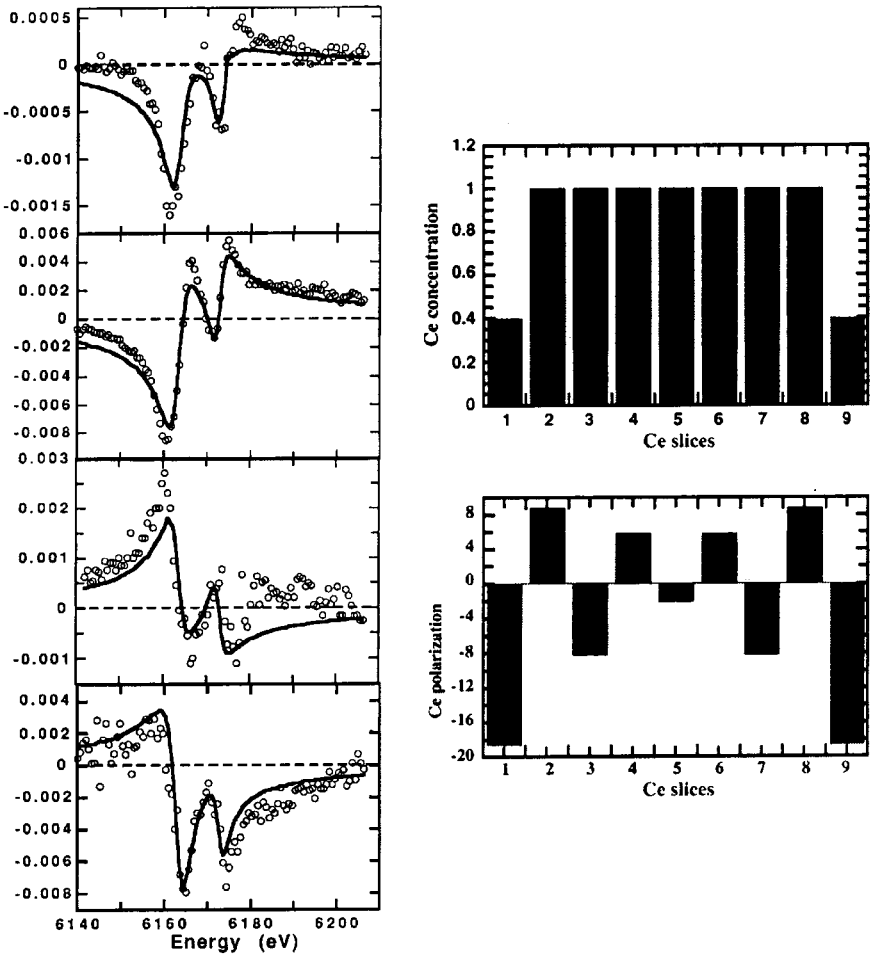

Figure 29. Energy dependence of the magnetic reflection intensity of a Ce_{22}/Fe_{30} multilayer, corrected for absorption, at the cerium L_{II} edge (a): (○) experimental values and (—) the best simulations obtained using the Ce concentration and the oscillating magnetic profile shown in (b). (Reprinted with permission from ref 165. Copyright 1999 American Physical Society.)

gated. Furthermore, as resonant X-ray diffraction contains the long-range order structural information, it can separate different magnetic contributions in the sample. For example, in Ce/Fe multilayers, X-ray magnetic circular dichroism experiments at the L and M edges show that the hybridization of the Ce *5d* and *4f* states with the *3d* states at the Fe interface induces magnetic ordering at room temperature, with a weak magnetic moment on both the *5d* and *4f* states of Ce. Using a circular polarization of the X-ray beam, scattering measurements performed with the magnetic field applied parallel or antiparallel to the diffraction plane display a difference or asymmetry ratio which can be interpreted only by the existence of an oscillating polarization distribution for Ce (Figure 29). Such complex magnetic structural arrangements can be detected only by resonant scattering methods, thus demonstrating their usefulness for defining X-ray magnetic spectroscopy results.[165] As a result, this method is used in the soft X-ray energy range to study artificially structured magnetic devices[166−168] and in hard X-ray for more classic magnetic samples.[169−172] The use of X-rays for structural magnetic studies is today a very well-established technique that is complementary to those involving neutrons.

IX. Experimental Requirements for Resonant Diffraction

Resonant diffraction experiments are based on variations of the f_a' and f_a'' anomalous factors, which are much weaker than that of the Thomson scattering. Consequently, DAFS, MAD, and resonant experiments must be accurate. They have special requirements both for the experimental setup and for the data collection process, where several sources of systematic errors must be avoided.

(i) For MAD and contrast experiments, the energy stability is crucial to get reliable values of f_a' and f_a''. Furthermore, a high-energy resolution increases the f_a'/f_a'' loop area and improves the phasing power. This means that third-generation sources are well suited for such experiments (source stability, high flux which allows high energy resolution).

(ii) For DAFS experiments, precise energy calibration is necessary. In mixed-valence samples, cations in different sites could give spectra that differ only by a small energy shift (1−2 eV). When several reflections are measured successively at each energy, this source of error decreases. However, in all cases an external check is needed. The best way is to measure directly, in fluorescence mode, either the

beam scattered by air through a metal foil or the absorption of the sample itself.[118,173] In this last case, the absorption reference used is that of the sample: the energy resolution of the absorption spectrum and the DAFS ones are identical.

(iii) For anomalous measurements performed in dispersive diffraction mode, raw $I(E)$ spectra must be normalized by the incident beam intensity $I_0(E)$, spatial distortions, and intensity responses of different pixels of the 2D detector. For the data analysis, a pixel/energy calibration must be performed carefully. For DAFS measurements, the sample to detector distance is strictly constant, and a single XAFS spectrum recorded on the same detector in transmission geometry with a powder sample can be used for this energy calibration.[174]

(iv) When the sample is bathed into the beam, an additional beam monitor is needed. Even when very small slits are used, due to the confusion sphere of the goniometer, their sizes must be always slightly larger than the sample dimension and the crystal receives only part of the monitored beam. If the beam intensity distribution is not perfectly homogeneous and varies with energy, errors due to standard monitors will be larger than the DAFS oscillations. A scintillation detector, mounted on the diffractometer, can measure fluorescence from the crystal as the energy is scanned through the absorption edge and at each energy we can have a continuous check of any discontinuity in the incident beam intensity received by the sample itself.[118]

(v) As anomalous measurements are performed at absorption edges, the scattered intensity must be first corrected for the total absorption effects. As absorption correction can be sensitive to variations in thickness of a few micrometers, only the surface of the sample diffracts and an accurate absorption correction must be used for highly absorbing powders.[175] For single crystals, the absorption correction is highly sensitive to crystal shape and must take precisely into account the crystal geometry. An accurate empirical absorption correction procedure was developed by Vacinova et al.[118] to take this effect into account.

Furthermore, compared with XAFS measurements, DAFS and anisotropy experiments are synchrotron beam time-consuming since they correspond to absorption measurements performed on a diffraction peak. For this reason different experimental modes of resonant data collection have been developed: (i) *multimonochromatic diffraction* (MMD), which is performed with classical monochromatic optics, and (ii) *dispersive diffraction* (DD), which uses energy-dispersive optics.

In the DD mode, the incident beam angle distribution $\Delta\alpha$ in the horizontal plane is directly correlated to the photon energy distribution[176] and several raw diffracted spectra $I(E)$ are collected simultaneously on the 2D-detector (Figure 30). This DD mode was first proposed for phase determination by Arndt et al.[177] Despite a large gain in time obtained for the collection of $I(E)$ spectra, several subsequent experiments show possibilities but also difficulties of this mode for resonant diffraction and DAFS experiments.[178−180] Most difficulties in the quantitative data analysis are discussed and solved through a new integration procedure "DAD".[66] However, energy resolution of DD data is intrinsically limited by the sample mosaicity and data quality is worse than that obtained on the MMD mode. The DD technique could, yet, prove valuable for in-situ experiments under variable external conditions and for *simultaneous-MAD* experiments.[65,99]

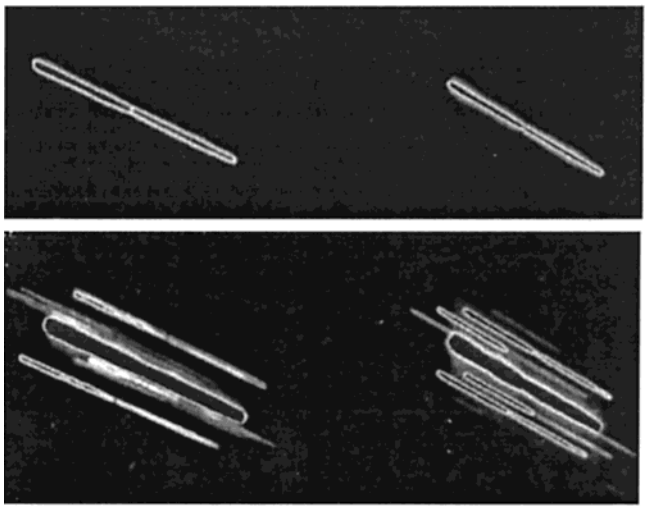

Figure 30. 2D-DAFS spectra of two reflections and their eight incommensurate satellites, measured at the tantalum L_{III} edge on the $(TaSe_4)_2I$ crystal, above and below the Peierls transition at 263 K. The length of each reflection is directly related to the angular span of the dispersive beam and the Bragg angle variation with energy. The Ta L_{III} absorption edge can be seen at the middle of the diffracted lines. (Reprinted with permission from ref 99. Copyright 1999 Université Joseph Fourier, Grenoble.)

Up to now, nearly all resonant experiments have been performed in the multimonochromatic diffraction mode with traditional monochromatic optics. Diffracted intensities could be measured using an omega-scan that integrates the reflection. This is required for compounds with ill-shaped reflection profiles due to the mosaic spread and/or the domain structure.[118] This procedure must be done for all energies and therefore is time-consuming. This omega-scan is, however, not needed when the reflection profile is well defined and relatively broad. In this case, the exact Bragg angle of the reflection at each energy can be calculated and the intensity data collection can be performed only at the top of this reflection or with a limited sample oscillation.[114,117,122,181,182] DAFS data acquisition using the MMD mode is now well established and accurate. Extended DAFS spectra, satisfying the criteria of the XAFS community, can be obtained at different synchrotron radiation facilities. This means that with this MMD mode we can measure Bragg reflection intensities as a function of the energy with an accuracy better than 0.5%.

X. Conclusions

It could be said that nowadays resonant diffraction can be used to determine any information about any element in a crystal: phase of its structure factor,

valence, neighbors, orbital characteristics, magnetic properties, etc. However, all of these information have a price: they require a sophisticated tool (synchrotron rings) as well as a complex analysis. However, thanks to efforts of the scientific community, several straightforward applications are now available.

The first one concerns the (long-expected) availability of an experimental determination of the phase. This method (MAD) is vital for the structure determination of complex macromolecules for which direct methods are helpless. The software dedicated to these studies, as well as technical developments (cryocooling, 2D detectors), and the worldwide availability of synchrotron radiation have made this method a well established one, routinely used by structural biologists.[183] Speed and availability of beam time is also becoming less relevant: specialized beam lines providing high intensity and fast detectors can yield complete, three-wavelengths, MAD data collection in less than half an hour.[184]

The second type of application uses more directly the chemical sensitivity of resonant diffraction and is more relevant for inorganic materials: it is possible to extract the contribution of a single element in a given crystallographic site. Even if this method is less used than the MAD one, it is also a well-established one for analyses of complex substituted powders. It can thus be used to distinguish elements having a close scattering power (contrast) with much less material required compared to neutron diffraction. Furthermore, resonant X-ray analyses can be performed on a single sample, without any isotopic replacement as needed for neutron experiments.

Also interesting to the chemist should be the DAFS method: the fine structure of the intensity as a function of the energy is directly related to the valence, the anisotropy, and the coordination of the resonant atom. However, like the resonant magnetic scattering, this last technique requires an important beam time to allow the collection of energy spectra for several reflections. Even if softwares have been developed for the analysis of such experiments, the improvement of data collection speed and the development of more dedicated software for an easier analysis is now the goal of researchers in this field. This is a price that still needs to be entirely paid to fully extract the rich "*anomalous*" information.

XI. Acknowledgments

Authors acknowledge J. Vacinova, S. Grenier, P. Wolfers, D. E. Cox, M. G. Proietti, J. Garcia, G. Subias, W. Shepard, M. Hagelstein, A. San Miguel, T. Neisius, S. Pascarelli, B. Ravel, L. Seve, J. M. Tonnerre, F. de Bergevin, and D. Raoux for helpful collaborations, discussions, and/or support on resonant scattering studies. They also acknowledge E. Geissler and R. Kahn for critically reading this manuscript. Finally, they dedicate this contribution to the memory of L. Seve who unexpectedly deceased in February 2000.

XII. References

(1) Mark, H.; Szillard, L. *Z. Phys.* **1925**, *33*, 688.
(2) Bradley, A. J.; Rodgers, J. W. *Proc. R. Soc.* **1934**, *A144*, 340.
(3) Jones, F. W.; Sykes, C. *Proc. R. Soc.* **1937**, *A161*, 440.
(4) Coster, D.; Knol, K. S.; Prins, J. A. *Z. Phys.* **1930**, *63*, 345.
(5) Bijvoet, J. M. *Proc. Acad. Sci. Amsterdam* **1949**, *B52*, 313.
(6) Cauchois, Y. *C. R. Acad. Sci.* **1956**, *242*, 100.
(7) *Anomalous scattering*; Ramaseshan, S., Abrahams, S. C., Eds.; Munsksgaard: Copenhagen, 1975.
(8) *Resonant anomalous X-ray scattering*; Materlink, G., Sparks, C. J., Fischer, K., Eds.; Elsevier Science B.V.: Amsterdam, 1994.
(9) Kissel, L.; Pratt, R. H. *Acta Crystallogr.* **1990**, *A46*, 170.
(10) James, R. W. *The optical principles of the diffraction of X-rays*; Cornell University Press: Ithaca, NY, 1965. Ox Box Press: Woodbridge, CT, 1982.
(11) Toll, J. *Phys. Rev.* **1956**, *104*, 1760.
(12) Bergstrom, P. M., Jr.; Kissel, L.; Pratt, R. H.; Costescu, A. *Acta Crystallogr.* **1997**, *A53*, 7.
(13) Suortti, P.; Hasting, J. B.; Cox, D. E. *Acta Crystallogr.* **1985**, *A41*, 413.
(14) Hendrickson, W. A. *Science* **1991**, *254*, 51.
(15) Cromer, D. T.; Liberman, D. *J. Chem. Phys.* **1970**, *53*, 1891.
(16) Chantler, C. T. In *Resonant anomalous X-ray scattering*; Materlink, G., Sparks, C. J., Fischer, K., Eds.; Elsevier Science B. V.: Amsterdam, 1994; p 61.
(17) Sasaki, S. *Tables*; National Laboratory for High Energy Physics Report, Tsukuba, Japan, 1984.
(18) Henke, B. L.; Gullikson, E. M.; Davis, J. C. *At. Data, Nucl. Data Tables* **1993**, *54*, 181.
(19) Brown, M.; Peierls, R. E.; Stern, E. A. *Phys. Rev.* **1977**, *B15*, 738
(20) Coppens, P. *Synchrotron Radiation Crystallography*; Academic Press: London, 1992; p 306.
(21) Krause, M. O.; Oliver, J. H. *J. Phys. Chem. Ref. Data* **1979**, *8*, 329.
(22) Arp, U.; Materlink, G.; Meyer, M.; Richter, M. In *X-ray Absorption Fine Structure*; Hasnain, S. S., Ed.; Ellis Horwood: New York, 1991; p 44.
(23) Wong, J.; Lytle, F. W.; Messmer, R. P.; Maylotte, D. H. *Phys. Rev.* **1984**, *B30*, 5596.
(24) *Theory and computation for synchrotron radiation spectroscopy*; Benfatto, M., Natoli, C. N.,; Pace, E., Eds.; AIP: New York, 2000.
(25) Fontaine, A. In *Neutrons and synchrotron radiation for condensed matter studies*, HERCULES courses Vol. I; Baruchel, J., Hodeau, J. L., Lehmann, M. S., Regnard, J. R., Schlenker, C., Eds.; Editions de Physique, les Ulis & Sringer-Verlag: Berlin, 1993; p 323.
(26) Brouder, C. *J. Phys.: Condens. Matter.* **1990**, *2*, 701 and references therein
(27) Templeton, D. H.; Templeton, L. K. *Acta Crystallogr.* **1980**, *A36*, 237.
(28) Templeton, D. H.; Templeton, L. K. *Acta Crystallogr.* **1982**, *A38*, 62.
(29) Templeton, D. H. In *Resonant anomalous X-ray scattering*; Materlink, G., Sparks, C. J., Fischer, K., Eds.; Elsevier Science B.V.: Amsterdam, 1994; p 1.
(30) Dmitrienko, V. E. *Acta Crystallogr.* **1983**, *A39*, 29. Dmitrienko, V. E. *Acta Crystallogr.* **1984**, *A40*, 89
(31) Blume, M. In *Resonant anomalous X-ray scattering*; Materlink, G., Sparks, C. J., Fischer, K., Eds.; Elsevier Science B.V.: Amsterdam, 1994; p 495.
(32) *Magnetism and synchrotron radiation*; Mittelwihr courses; Beaurepaire, E., Carrière, B., Kappler, J. P., Eds.; Editions de Physique: les Ulis, 1997.
(33) Templeton, L. K. Templeton, D. H. *J. Appl. Crystallogr.* **1988**, *21*, 558.
(34) Vacinova. J. Ph.D. Thesis, Grenoble University, 1997.
(35) Quintana, J. P.; Butler, B. D.; Haeffner, D. R. *J. Appl. Crystallogr.* **1991**, *24*, 184.
(36) Templeton, D. H.; Templeton, L. K.; Phillips, J. C.; Hodgson, K. O. *Acta Crystallogr.* **1980**, *A36*, 436.
(37) Freund, A. In *Anomalous scattering*; Ramaseshan, S., Abrahams, S. C., Eds.; Munksgaard: Copenhagen, 1975; p 69.
(38) Lengeler, B. In *Resonant anomalous X-ray scattering*; Materlink, G., Sparks, C. J., Fischer, K., Eds.; Elsevier Science B.V.: Amsterdam, 1994; p 35.
(39) Fukamachi, T.; Hosoya, S.; Kawamura, T.; Hunter, S.; Nakano, Y. *Jpn. J. Appl. Phys.* **1978**, *17*, 326.
(40) Stanglmeier, F.; Lengeler, B.; Weber, W.; Göbel, H.; Schuster, M. *Acta Crystallogr.* **1992**, *A48*, 626.
(41) Sève, L.; Tonnerre, J. M.; Raoux, D. *J. Appl. Crystallogr.* **1998**, *31*, 700.
(42) Hoyt, J. J.; DeFontaine, D.; Warburton, W. K. *J. Appl. Crystallogr.* **1984**, *17*, 344.
(43) Bonse, U.; Hartmann-Lotsch, I.; Lotsch, H. *Nucl. Instrum. Methods* **1983**, *172*, 224. Bonse, U.; Hartmann-Lotsch, I.; Lotsch, H. In *Near edge structures*; Bianconi, A., et al. Eds.; Chemical Physics Springer Series; Springer-Verlag: New York, 1983; p 27.
(44) Karle, J. *Phys. Today* **1989**, *June*, 22.

(45) Fourme, R.; Hendrickson, W. A. In *Biophysics and Synchrotron Radiation*; Hasnain, S., Horwood, A., Eds.; Chichester, U.K., 1990; p 156
(46) Helliwell, J. R. *Macromolecular Crystallography with Synchrotron Radiation*; Cambridge University Press: London, 1992.
(47) Fourme, R.; Shepard, W.; Schiltz, M.; Ramin, M.; Kahn, R. In *Structure and Dynamics of Biomolecules*; HERCULES courses Vol. IV; Fanchon, E., Geissler, E., Hodeau, J. L., Regnard, J. R., Timmins, P., Eds.; Oxford University Press: Oxford, 2000; p 36.
(48) Okaya, Y.; Pepinsky, R. *Phys. Rev.* **1956**, *103*, 1645.
(49) Peerdeman, A. F.; Bijvoet, J. M. *Acta Crystallogr.* **1956**, *9*, 1012.
(50) Mitchell, C. M. *Acta Crystallogr.* **1957**, *10*, 475.
(51) Hendrickson, W. A.; Teeter, M. M. *Nature* **1981**, *290*, 107.
(52) Karle, J. *Int. J. Quantum Chem.* **1980**, *7*, 357.
(53) Hendrickson, W. A. *Trans. Am. Crystallogr. Assoc.* **1985**, *21*, 11.
(54) Kahn, R.; Fourme, R.; Bosshard, R.; Chiadmi, M.; Risler, J. L.; Dideberg, O.; Wery, J. P. *FEBS Lett.* **1985**, *179*, 133.
(55) Guss, J. M.; Merritt, E. A.; Phizackerley, R. P.; Hedman, B.; Murata, M.; Hodgson, K. O.; Freeman, H. C. *Science* **1988**, *241*, 806.
(56) Peterson, M. R.; Harrop, S. J.; McSweeney, S. M.; Leonard, G. A.; Thompson, A. W.; Hunter, W. N.; Helliwell, J. R. *J. Synchrotron Radiat.* **1996**, *3*, 24.
(57) Shepard, W.; Cruse, W. B. T.; Fourme, R.; de la Fortelle, E.; Prangé, T. *Structure* **1998**, *6*, 849.
(58) Hendrickson, W. A.; Smith, J. L.; Phizackerley, R. P.; Merritt, E. A. *Proteins* **1988** *4*, 77.
(59) Weis, W. I.; Kahn, R.; Fourme, R.; Drickamer, K.; Hendrickson, W. A. *Science* **1991**, *254*, 1608.
(60) Burling, F. T.; Weis, W. I.; Flaherty, K. M.; Brünger, A. T. *Science* **1996**, *271*, 72.
(61) Hendrickson, W. A.; Horton, J. R.; LeMaster, D. M. *EMBO J.* **1990**, *9*, 1665.
(62) Phillips, J. C.; Hodgson, K. O. *Acta Crystallogr.* **1980**, *A36*, 856.
(63) Iwasaki, H.; Yurugi, T.; Yoshimura, Y. *Acta Crystallogr.* **1999**, *A55*, 864.
(64) Lee, P. L.; Ogata, C. M. *J. Appl. Crystallogr.* **1995**, *28*, 661.
(65) Shepard, W.; Favre-Nicolin, V.; Chesne, M. L.; Abergel, C.; Bos, S.; Chantalat, L.; Kahn, R.; Lorenzo, E.; Natali, F.; Neisius, T.; Pascarelli, S.; Vicat, J.; Hodeau, J. L. ECM19 Conference, Nancy, France, 2000.
(66) Favre-Nicolin, V.; Bos, S.; Lorenzo, E.; Bordet, P.; Shepard, W.; Hodeau, J. L. *J. Appl. Crystallogr.* **2000**, *33*, 52.
(67) Hendrickson, W. A.; Ogata, C. M. *Methods Enzymol.* **1997**, *276*, 494.
(68) Cross, J. O.; Newville, M. G.; Rehr, J. J.; Sorensen, L. B.; Bouldin, C. E.; Watson, G.; Gouder, T.; Lander, G. H.; Bell, M. I. *Phys. Rev.* **1998**, *B58*, 11215.
(69) Kahn, R.; Carpentier, P.; Berthet-Colominas, C.; Capitan, M.; Chesne, M. L.; Fanchon, E.; Lequien, S.; Thiaudière, D.; Vicat, J.; Zielinski, P.; Stuhrmann, H. *J. Synchrotron Radiat.* **2000**, *7*, 131.
(70) Prandl, W. *Acta Crystallogr.* **1990**, *A46*, 988.
(71) Limper, W.; Prandl, W.; Wroblewski, T. *Mater. Sci. Forum* **1991**, *79*−*82*, 221.
(72) Attfield, J. P. *Mater. Sci. Forum* **1996**, *228*−*231*, 201.
(73) Heger, G. In *Neutron and Synchrotron Radiation for Condensed Matter Studies*; HERCULES courses Vol. II; Baruchel, J., Hodeau, J. L., Lehmann, M. S., Regnard, J. R., Schlenker, C., Eds.; Editions de Physique, les Ulis−F & Springer-Verlag: Heidelberg, 1994; p 23.
(74) Cox, D.; Wilkinson, A. P. In *Resonant anomalous X-ray scattering*; Materlink, G., Sparks, C. J., Fischer, K., Eds.; Elsevier Science B.V.: Amsterdam, 1994; p 195.
(75) Howland, R. S.; Geballe, T. H.; Laderman, S. S.; Fisher-Colbrie, A.; Scott, M.; Tarascon, J. M.; Barboux, P. *Phys Rev.* **1989**, *B39*, 9017.
(76) Lorimier, J. Ph.D. Thesis, Dijon University, 2000.
(77) Wilkinson, A. P.; Cheetham, A. K.; Tang, S. C.; Reppart, W. J. *Chem. Commun.* **1992**, 1485.
(78) Nelmes, R. J.; Hatton, P. D.; McMahon, M. I.; Piltz, R. O.; Crain, J.; Cernik; R. J.; Bushnell-Wye, G. *Rev. Sci. Instrum.* **1992**, *63*, 1039.
(79) Wulf, R. *Acta Crystallogr.* **1990**, *A46*, 681.
(80) Kitagawa, Y.; Tanaka, N.; Hata, Y.; Katsube, Y.; Satow, Y. *Acta Crystallogr.* **1987**, *B43*, 272.
(81) Tsukimura, K.; Sasaki, S.; Ohashi, H. *Acta Crystallogr.* **1990**, *B46*, 493.
(82) Helliwell, M.; Helliwell, J. R.; Kaucic, V.; Zabukovec Logar, N.; Barba, L.; Busetto, E.; Lausi, A. *Acta Crystallogr.* **1999**, *B55*, 327.
(83) de Santis, M.; de Andres, A.; Raoux, D.; Maurer, M.; Piecuch, M.; Ravet, M. *Phys Rev.* **1992**, *B46*, 15465.
(84) Déchelette, A.; Saint-Lager, M. C.; Tonnerre, J. M.; Patrat, G.; Raoux, D.; Fischer, H.; Andrieu, S.; Piecuch, M. *Phys. Rev.* **1999**, *B60*, 6623.
(85) Williams, A.; Kwei, G. H.; Ortiz, A. T.; Karnowski, M.; Warburton, W. K. *J. Mater. Res.* **1990**, *5*, 1197.
(86) Warner, J. K.; Wilkinson, A. P.; Cheetham, A. K.; Cox, D. E. *J. Phys. Chem. Solids* **1991**, *52*, 1251.
(87) Reimer, W.; Hellner, E.; Treutmann, W.; Heger, G. *J. Phys. C: Solid State Phys.* **1982**, *15*, 3597.
(88) Aranda, M. A. G.; Sinclair, D. C.; Attfield, J. P.; Mckenzie, A. P. *Phys. Rev.* **1995**, *B51*, 12747.
(89) Kwei, G. H.; Von Dreele, R. B.; Cheong, S. W.; Fisk, Z.; Thompson, J. D. *Phys. Rev.* **1990**, *B41*, 1889.
(90) Coppens, P.; Lee, P.; Gao, Y.; Sheu, H. S. *J. Phys. Chem. Solids* **1991**, *52*, 1267.
(91) Marcos, M. D.; Aranda, M. A. G.; Sinclair, D. C.; Attfield, J. P. *Physica C* **1994**, *C235*−*240*, 967.
(92) Joubert, J. M.; Cerny, R.; Latroche, M.; Percheron-Gueguan, A.; Yvon, K. *J. Appl. Crystallogr.* **1998**, *31*, 327.
(93) Latroche, M.; Joubert, J. M.; Percheron-Gueguan, A.; Notten., P. H. L. *J. Solid State Chem.* **1999**, *146*, 313.
(94) Sinclair, D. C.; Aranda, M. A. G.; Attfield, J. P.; Rodriguez-Carvajal, J. *Physica C* **1994**, *225*, 307.
(95) Moroney, L. M.; Thompson, P.; Cox, D. E. *J. Appl. Crystallogr.* **1988**, *21*, 206.
(96) Moudden, A. H.; Durand, D.; Bessiere, M.; Lefebvre, S. *Phys. Rev.* **1988**, *B37*, 7655.
(97) Soejima, Y.; Yamasaki, K.; Fischer, K. F. *Acta Crystallogr.* **1997**, *B53*, 7655.
(98) Favre-Nicolin, V.; Bos, S.; Lorenzo, E.; Hodeau, J. L.; Berar, J. F.; Monceau, P.; Currat, R. *Phys. Rev. Lett.* **2001**, accepted for publication.
(99) Favre-Nicolin, V. Ph.D. Thesis, Grenoble University, 1999.
(100) Hashimoto, S.; Iwasaki, H.; Ohshima, K.; Harada, J.; Sakata, M. Terauchi, H. *J. Phys. Soc. Jpn.* **1985**, *54*, 3796.
(101) Ice, G. E.; Sparks, C. J. In *Resonant anomalous X-ray scattering*; Materlink, G., Sparks, C. J., Fischer, K., Eds.; Elsevier Science B.V.: Amsterdam, 1994; p 265.
(102) Simon, J. P.; Lyon, O.; De Fontaine, D. *J. Appl. Crystallogr.* **1985**, *18*, 230.
(103) Fuoss, P. H.; Eisenberger, P.; Warburaton, W. K.; Bienenstock, A. *Phys Rev. Lett.* **1981**, *46*, 1537.
(104) Matsubara, E.; Waseda, Y. In *Resonant anomalous X-ray scattering*; Materlink, G., Sparks, C. J., Fischer, K., Eds.; Elsevier Science B.V.: Amsterdam, 1994; p 345.
(105) Tonnerre, J. M.; de Lima, J. C.; Raoux, D. *J. Chim. Phys.* **1989**, *86*, 1509.
(106) Raoux, D. In *Resonant anomalous X-ray scattering*; Materlink, G., Sparks, C. J., Fischer, K., Eds.; Elsevier Science B.V.: Amsterdam, 1994; p 323.
(107) Meneghini, C.; Gualtieri, A. F.; Siligardi, C. *J. Appl. Crystallogr.* **1999**, *32*, 1090.
(108) Liang, K. S.; Laderman, S. S.; Sinfelt, J. H. J. *Chem. Phys.* **1987**, *86*, 2352.
(109) Sayers, D.; Renevier, H.; Hodeau, J. L.; Berar, J. F.; Tonnerre, J. M.; Raoux, D.; Chester, A.; Bazin, D.; Bouldin, C. E. *ESRF Newsl.* **1997**, *janv.*, 18.
(110) Cauchois, Y.; Bonnelle, C. *C. R. Acad. Sci.* **1956**, *242*, 1596.
(111) Heno, Y. *C. R. Acad. Sci.* **1956**, *242*, 1599.
(112) Fukamachi, T. S.; Hosoya, S.; Kawamura, T.; Hastings, J. *J. Appl. Crystallogr.* **1977**, *10*, 321.
(113) Arcon, I.; Kodre, A.; Glavic, D.; Hribar, M. *J. Phys.* **1987**, *C9*, 1105 1987.
(114) Stragier, H.; Cross, J. O.; Rehr, J. J.; Sorensen, L. B.; Bouldin, C. E.; Woicik, J. C. *Phys. Rev. Lett.* **1992**, *21* 3064.
(115) Pickering, I. J.; Sansone, M.; March, J.; George, G. N. *J. Am. Chem. Soc.* **1993**, *115*, 6302.
(116) Sorensen, L. B.; Cross, J. O.; Newville, M.; Ravel, B.; Rehr, J. J.; Stragier, H.; Bouldin, C. E.; Woicik, J. C. In *Resonant anomalous X-ray scattering*; Materlink, G., Sparks, C. J., Fischer, K., Eds.; Elsevier Science B.V.: Amsterdam, 1994; p 389.
(117) Renevier, H.; Hodeau, J. L.; Wolfers, P.; Andrieu, S.; Weigelt, J.; Frahm, R. *Phys. Rev. Lett.* **1997**, *78*, 2775.
(118) Vacínová, J.; Hodeau, J. L.; Wolfers, P.; Lauriat, J. P.; Elkaïm, E. *J. Synchrotron Radiat.* **1995**, *2*, 236.
(119) Qing Ma; Sayers, D. *Physica B* **1995**, *B208*−*209*, 224.
(120) Hodeau, J. L.; Vacínová, J. *Synchrotron Radiat. News* **1996**, *9*, 15.
(121) Meyer, D. C.; Richter, K.; Seidel, A.; Weigelt, J.; Frahm, R.; Paufler, P. *J. Synchrotron Radiat.* **1998**, *5*, 1275.
(122) Proietti, M. G.; Renevier, H.; Hodeau, J. L.; Garcia, J., Berar, J. F.; Wolfers, P. *Phys. Rev.* **1999**, *B59*, 5479.
(123) Woicik, J. C.; Cross, J. O.; Bouldin, C. E.; Ravel, B.; Pellegrino, J. G.; Steiner, B.; Bompadre, S. G.; Sorensen, L. B.; Miyano, K. E.; Kirkland, J. P. *Phys. Rev.* **1998**, *B58*, R4215.
(124) Ravel, B.; Bouldin, C. E.; Renevier, H.; Hodeau, J. L.; Berar, J. F. *Phys Rev.* **1999**, *B60*, 778.
(125) Hodeau, J. L.; Vacínová, J.; Garreau, Y.; Fontaine, A.,; Elkaïm, E.; Lauriat, J. P.; Hagelstein, M.; Muller, J.; Collomb, A. *Nucl. Instrum. Methods* **1995**, *B97*, 115.
(126) Renevier, H.; Weigelt, J.; Andrieu, S.; Frahm, R.; Raoux, D. *Physica B* **1995**, *B208*−*209*, 217.

(127) Frenkel, A. I.; Fanning, D. M.; Robinson, I. K.; Adler, D. L.; Cross, J. O. In *First principles calculations for ferroelectrics*; Cohen, R. E., Ed.; 1998; p 96.
(128) Attfield, J. P. *Nature* **1990**, *343*, 46.
(129) Wilkinson, A. P.; Cheetham, A. K. *J. Appl. Crystallogr.* **1992**, *25*, 654.
(130) Gao, Y.; Pressprish, M. R.; Coppens, P. *Acta Crystallogr.* **1993**, *A49*, 216.
(131) Kwei, G. H.; Von Dreele, R. B.; Williams, A.; Goldstone, J. A.; LawsonII, A. C.; Warburton, W. K. *J. Mol. Struct.* **1990**, *223*, 383.
(132) Vacínová, J.; Hodeau, J. L. *J. Solid State Chem.* **1998**, *140*, 201.
(133) Cross, J. O.; Newville, M.; Sorensen, L. B.; Stragier, H. J.; Bouldin, C. E.; Woicik, J. C. *J. Phys. IV* **1997**, *7(C2)*, 745.
(134) Wilkinson, A. P.; Cheetham, A. K.; Cox, D. E. *Acta Crystallogr.* **1991**, *B47*, 155.
(135) Bos, S.; Favre-Nicolin, V.; Lorenzo, E.; Renevier, H.; Hodeau, J. L.; Cajipe, V.; Leone, P.; Gueho, C.; Vaughan, G. XVII European Phys. Conf., Grenoble, France, 1998.
(136) Vacinova, J.; Hodeau, J. L.; Bordet, P.; Anne, M.; Cox, D.; Fitch, A.; Pattison, P.; Schweggle, W.; Graafsma, H.; Kvick, A. *Mater. Sci. Forum* **1996**, *228−231*, 241.
(137) Templeton, D. H.; Templeton, L. K. *Acta Crystallogr.* **1985**, *A41*, 365.
(138) Wilkinson, A. P.; Templeton, L. K.; Templeton, D. H. *J. Solid State Chem.* **1995**, *118*, 383.
(139) Templeton, D. H.; Templeton, L. K. *Acta Crystallogr.* **1989**, *A45*, 39.
(140) Templeton, D. H.; Templeton, L. K. *Acta Crystallogr.* **1986**, *A42*, 478.
(141) Templeton, D. H.; Templeton, L. K. *Acta Crystallogr.* **1987**, *A43*, 573.
(142) Kirfel, A.; Petcov, A. *Acta Crystallogr.* **1992**, *A48*, 247.
(143) Kirfel, A. In *Resonant anomalous X-ray scattering*; Materlink, G., Sparks, C. J., Fischer, K., Eds.; Elsevier Science B.V.: Amsterdam, 1994; p 231.
(144) Finkelstein, K. D.; Hamrick, M.; Shen, Q. In *Resonant anomalous X-ray scattering*; Materlink, G., Sparks, C. J., Fischer, K., Eds.; Elsevier Science B.V.: Amsterdam, 1994; p 91.
(145) Kokubun, J.; Nagano, T.; Kuribayashi, M., Ishida, K. *J. Phys. Soc. Jpn.* **1998**, *67*, 3114.
(146) Benfatto, M.; Joly, Y.; Natoli, C. R.*Phys. Rev. Lett.* **1999**, *83*, 636.
(147) Dmitrienko, V. E.; Ovchinnikova, E. N. *Acta Crystallogr.* **2000**, *A56*, 340.
(148) Fabrizio, M.; Altarelli, M.; Benfatto, M. *Phys. Rev. Lett.* **1998**, *80*, 3400.
(149) Paolasini, L.; Vettier, C.; de Bergevin, F.; Yakhou, F.; Mannix, D.; Stunault, A.; Neubeck, N.; Altarelli, M.; Fabrizio, M.; Metcalf, P. A.; Honig, J. M. *Phys. Rev. Lett.* **1999**, *82*, 4719.
(150) Ovchinnikova, E. N.; Dmitrienko, V. E. *Acta Crystallogr.* **2000**, *A56*, 2.
(151) Hagiwara, K.; Kanazawa, M.; Horie, K.; Kokubun, J.; Ishida, K. *J. of Phys. Soc. Jpn.* **1999**, *68*, 88.
(152) Garcia, J.; Subias, G.; Proietti, M. G.; Renevier, H.; Joly, Y.; Hodeau, J. L.; Blasco, J.; Sanchez, M. C.; Berar, J. F. *Phys. Rev. Lett.* **2000**, *85*, 578.
(153) Mach, P.; Pindak, R.; Levelut, A. M.; Barois, P.; Nguyen, H. T.; Huang, C. C.; Furenlid, L. *Phys. Rev. Lett.* **1998**, *81*, 1015.
(154) Mach, P.; Pindak, R.; Levelut, A. M.; Barois, P.; Nguyen, H. T.; Baltes, H.; Hird, M.; Toyne, K.; Seed, A.; Goodby, J. W.; Huang, C. C.; Furenlid, L. *Phys. Rev.* **1999**, *E60*, 6793.
(155) Levelut, A. M.; Pansu, B. *Phys. Rev.* **1999**, *E60*, 6803.
(156) Fanchon, E.; Hendrickson, W. A. *Acta Crystallogr.* **1990**, *A46*, 809.
(157) Schiltz, M.; Bricogne, G. X-ray Gyrotropy and Synchrotron Radiation based Chiroptical Spectroscopies Conference, Grenoble, France, Sept. 21−23 , 2000.
(158) Platzman, P. M.; Tzoar, N. *Phys. Rev.* **1970**, *B2*, 3536.
(159) de Bergevin, F.; Brunel, M. *Phys. Lett.* **1972**, *A39*, 141.
(160) Blume, M. *J. Appl. Phys.* **1985**, *57*, 3615.
(161) Gibbs, D.; Harshmann, D. R.; Isaacs, E. D.; McWhan, D. B.; Mills, D.; Vettier, C. *Phys. Rev. Lett.* **1988**, *61*, 1241.
(162) Hannon, J. P.; Trammell, G. T.; Blume, M.; Gibbs, D. *Phys. Rev. Lett.* **1988**, *61*, 1245.
(163) McWhan, D. B.; Vettier, C.; Isaacs, E. D.; Ice, G. E.; Siddons, D. P.; Hastings, J. B.; Peters, C.; Vogt, O. *Phys. Rev.* **1990**, *B42*, 6007.
(164) Vettier, C. In *Resonant anomalous X-ray scattering*; Materlink, G., Sparks, C. J., Fischer, K., Eds.; Elsevier Science B.V.: Amsterdam, 1994; p 513.
(165) Sève, L.; Jaouen, N.; Tonnerre, J. M.; Raoux, D.; Bartolomé, F.; Arend, M.; Felsch, W.; Rogalev, A.; Goulon, J.; Gautier, C.; Berar, J. F. *Phys. Rev.* **1999**, *B60*, 9662.
(166) Tonnerre, J. M.; Sève, L.; Raoux, D.; Soullié, G.; Rodmaq, B.; Wolfers, P. *Phys. Rev.* **1995**, *75*, 740.
(167) Tonnerre, J. M.; Sève, L.; Barbara-Dechelette, A.; Bartholomé, F.; Raoux, D.; Chakarian, V.; Kao, C. C.; Fischer, H.; Andrieu, S.; Fruchart, O. *J. Appl Phys.* **1998**, *83*, 6293.
(168) Sacchi, M.; Mirone, A. *Phys. Rev.* **1998**, *B57*, 8408.
(169) McWhan, D. B. *J. Synchrotron Radiat.* **1994**, *1*, 83 and references therein.
(170) Tang, C.; Stirling, W. G.; Lander, G. H.; Gibbs, D.; Herzog, W.; Carra, P.; Thole T.; Mattenberger, K.; Vogt, O. *Phys. Rev.* **1992**, *B46*, 5287.
(171) Hill, J. P.; Kao, C. C.; McMorrow, D. F. *Phys. Rev.* **1997**, *B55*, R8662.
(172) Gibbs, D.; Hill, J. P.; Vettier, C. *Phys. Status Solidi (b)* **1999**, *215*, 667.
(173) Cross, J. O.; Frenkel, A. I. *Rev. Sci. Instrum.* **1999**, *70*, 38.
(174) Bos, S. Ph.D. Thesis, Grenoble University, 1999.
(175) Ehrenberg, H.; Knapp, M.; Hartmann, T.; Fuess, H.; Wroblewski, T. *J. Appl. Crystallogr.* **2000**, *33*, 953.
(176) Matsushita, T.; Phizackerley, R. P. *Jpn. J. Appl. Phys.* **1981**, *20*, 2223.
(177) Arnd, U. W.; Greenhough, T. J.; Helliwell, J. R.; Howard, A. K.; Rule, S. A.; Thompson, A. W. *Nature* **1982**, *298*, 835.
(178) Rodricks, B.; Lamelas, F.; Medjahed, D.; Dos Passos, W.; Smither, R.; Ziegler, E.; Fontaine, A.; Clarke, R. *Mater. Res. Soc. Symp. Proc.* **1989**, *143*, 209.
(179) Hodeau, J. L.; Vacínová, J.; Garreau, Y.; Fontaine, A.,; Hagelstein, M.; Elkaïm, E.; Lauriat, J. P.; Prat, A.; Wolfers, P. *Rev. Sci. Instrum.* **1995**, *66*, 1499.
(180) Finkelstein, K. D.; Sutton, M. *Nucl. Instrum. Methods* **1994**, *A347*, 495.
(181) Cross, J. O.; Elam, W. T.; Harris, V. G.; Kirkland, J. P.; Bouldin, C. E.; Sorensen, L. B. *J. Synchrotron Radiat.* **1998**, *5*, 911.
(182) Meyer, D. C.; Gawlitza, P.; Richter, K.; Schulze, K. D.; Sprungk, R.; Paufler, P. *J. Synchrotron Radiat.* **1998**, *5*, 128.
(183) The CCP4 suite: programs for protein crystallography, Number 4 Collaborative Computational Project. *Acta Crystallogr.* **1994**, *D50*, 760.
(184) Walsh, M. A.; Dementieva, I.; Evans, G.; Sanishvili, R.; Joachimiak, A. *Acta Crystallogr.* **1999**, *D55*, 1168.

CR0000269